2015

Validation and application of close-range photogrammetry to quantify ephemeral gully erosion

Karl Richard Gesch
Iowa State University

Validation and application of close-range photogrammetry to quantify ephemeral gully erosion

by

Karl Richard Gesch

A thesis submitted to the graduate faculty

in partial fulfillment of the requirements for the degree of

MASTER OF SCIENCE

Major: Soil Science

Program of Study Committee:
Richard Cruse, Major Professor
Lee Burras
Mark Tomer

Iowa State University

Ames, Iowa

2015

TABLE OF CONTENTS

LIST OF TABLES

LIST OF FIGURES

LIST OF ABBREVIATIONS

AnnAGNPS	Annualized Agricultural Non-Point Source
CREAMS	Chemicals, Runoff, and Erosion from Agricultural Management Systems
DEM	digital elevation model
EAM	end area method
EGEM	Ephemeral Gully Erosion Model
EphGEE	Ephemeral Gully Erosion Estimator
GCP	ground control point
IaRTN	Iowa Real-Time Network
IDEP	Iowa Daily Erosion Project
LiDAR	light detection and ranging
MAE	mean absolute error
NN	nearest neighbor
RMS	root mean square
RMSE	root mean square error
RTK-GPS	real-time kinematic global positioning system
RUSLE2	Revised Universal Soil Loss Equation 2
SIFT	scale-invariant feature transform
VP	validation point
WEPP	Water Erosion Prediction Project

LIST OF SYMBOLS

B_b	bank, bottom
B_t	bank, top
Con	control
C_b	channel, bottom
C_t	channel, top
$\varepsilon_{\Delta Z}$	vertical change error
ΔM	mass flux
$\delta \Delta M$	mass flux uncertainty
μ	mean
ρ_b	bulk density
σ	sample standard deviation
T_i	time corresponding to i
ΔV	volume change
ΔV_c	total channel volume change
$\delta \Delta V$	volume change uncertainty
$\hat{Z}$	elevation difference
$\delta \Delta Z$	elevation change uncertainty
$\delta Z_{\text{geo-ref}}$	absolute vertical accuracy
δZ_{rel}	relative vertical accuracy

ACKNOWLEDGEMENTS

Many people have helped and encouraged me as I have explored the world of soil science. I am deeply grateful to Rick Cruse, not only for giving me an opportunity to pursue a graduate degree in soil science, but also for his guidance and friendship. Laura Peterson and Jon Jensen first opened my eyes to the importance of soil and agriculture. I would also like to thank Lee Burras for insightful conversations and Mark Tomer for always making me feel like a peer. My research would have been impossible if not for the patience, mentoring, and cooperation of Rob Wells, Henrique Momm, and Seth Dabney. I am both humbled and honored to have collaborated with such excellent scientists.

Chris Witte greatly facilitated field operations and helped with initial setup. Kevin Cole shared survey equipment and taught me how to use it. Jody Ohmacht shared time, expertise, and laboratory space to assist me with soil analysis. Tom Lawler and Kerry Culp also helped with soil analyses. I would like to express my gratitude to the other members of Rick's lab group: Scott Lee, Victoria Scott, Heidi Dittmer, Sarah Anderson, Natalia Rogovska, Melissa Miller, and Hao Li. Their assistance with fieldwork and sharing of ideas greatly improved this research project.

Finally, I am thankful to my parents, Dean and Amy, and my brother, Brian, for their love and encouragement, and I am grateful to my wife, Renee, for constantly showing her patience, support, and love.

ABSTRACT

Agricultural soil erosion is a serious problem on farms because it contributes to crop yield declines and beyond farms because it is a source of sediment and chemical pollutants. Ephemeral gullies effectively convey runoff and connect agricultural uplands to off-site waters, so control of this phenomenon would benefit multiple societal sectors. Soil conservationists often employ predictive soil erosion models to develop conservation plans, but commonly used models cannot account for ephemeral gully erosion. Future models with the capability to simulate such concentrated flow erosion must be verified with field measurements. This work sought to quantify the measurement uncertainty of a recently developed tool based on geo-referenced close-range digital photogrammetry and to apply it to naturally evolving channels in agricultural fields. Repeated photogrammetric surveys were conducted to create a set of point clouds, which were compared to define the two standard deviation (2σ) uncertainty in average elevation change between two point clouds as ± 1.29 to ± 2.55 mm (depending on surface relief), the 2σ relative vertical uncertainty of individual point clouds as 0.916 mm, and the 2σ geo-referenced vertical accuracy of entire point clouds as 8.26 cm. Utilization of the method at field monitoring sites resulted in average watershed-scale (0.47 to 3.19 ha) estimates of ephemeral gully erosion rates of 3.93, 0.847, and 0.415 Mg ha^{-1} for three time intervals during 2013 and 2014. For the average soil bulk density of approximately 1.2 Mg m^{-3}, the vertical change uncertainty applied to estimate soil mass moved by ephemeral gully erosion resulted in an average sediment flux uncertainty of ± 0.175 Mg. The small uncertainties determined in the validation study and the plausible rates of soil loss by topographically concentrated overland flow quantified in the field study reflect

the reliability of the data, which contributes to their utility for future refinement of soil erosion models that explicitly predict ephemeral gully erosion.

CHAPTER 1

IMPROVED MEASUREMENTS OF EPHEMERAL GULLY EROSION WILL ENHANCE SOIL CONSERVATION

Soil is the natural porous matrix of solid organic and mineral substances that exists at the surface of Earth. While sometimes considered discrete objects, soils are spatially and temporally continuous three-dimensional bodies that are dynamic in space and time (Schaetzl and Anderson, 2005). Soil occupies a critical zone known as the pedosphere in which the lithosphere, atmosphere, hydrosphere, and biosphere intersect and interact (Schaetzl and Anderson, 2005; Hillel, 2008). Due to this unique environmental position, soil provides the foundation for nearly all terrestrial life on Earth (Hillel, 2008). Soils are heterogeneous at multiple scales, and such complexity results in high diversity both among and within soils. The dynamism and biodiversity inherent in soil attest to its crucial yet delicate role in terrestrial ecosystems.

Properly functioning soil is capable of providing diverse ecosystem services such as human enjoyment, physical support for plants and human infrastructure, habitat for terrestrial biota, pest and waste control, climate regulation through biogeochemical fluxes, water storage and filtration, and the cycling and supplying of nutrients necessary for plant growth (Dominati et al., 2010; Hatfield et al., 2014). From the human perspective, one of the most important purposes of soil is its fundamental role in food production. In fact, natural systems – including soil – are intricately linked to anthropogenic systems through human activities such as agriculture (Cruse et al., 2014). Thus, agricultural management has profound impacts on natural entities such as soil. Soil management practices can either improve or worsen soil productivity (den Biggelaar et al., 2003b), where productivity is understood based on definitions suggested by Lal

(2001) and den Biggelaar et al. (2003a) to be the potential of soil to support biomass or energy production by some desired species or community of species. One typical consequence of soil mismanagement is accelerated soil erosion.

Physically, soil erosion is the translocation of surface soil particles. Such mass flux is the result of disequilibrium between opposing forces, i.e. work done on the soil system and the tendency of the soil to resist such work. Newton (1729) posited that a body at rest will thus remain unless force is exerted upon it. Accordingly, when energy in excess of some resistance threshold is applied to the soil surface, soil particles will move in response. Erosive agents that do work on the soil surface and initiate soil erosion include gravity, chemical reactions, physical forces of wind and water, and deliberate and accidental human disturbances (Lal, 2001). Each of these forces can cause substantial soil movement, but erosion by water has undergone much research due to its predominance in humid areas such as Iowa that are suitable for rain-fed agriculture. Agents of water erosion in uplands include soil pore flow, soil ice, raindrop impact, and runoff (Lal, 2001). Regardless of the erosive force, the three phases of soil erosion are detachment, transport, and deposition.

Soil erosion is a natural sub-process of soil formation and landscape development (e.g. Uri, 2000; Lal, 2001). Topsoil erosion is only one form of soil degradation (e.g. Lal, 2001; Hillel, 2008) but it is typically the most serious due to its irreversibility (Hillel, 2008). Johnson and Watson-Stegner (1987) asserted that pedogenesis includes regressive soil development. Thus, even though it involves degradation, erosion can be considered a pedogenic process. Despite this understanding, erosion is typically thought to counteract soil formation, which occurs due to inputs, outputs, internal mass fluxes, and material

alterations (Simonson, 1959) acting upon initial conditions over time (Jenny, 1941). On the human timescale of decades to centuries, soil erosion and soil genesis are indeed opposing processes because anthropogenically accelerated soil erosion rapidly outpaces pedogenesis.

Humans are capable of transporting tremendous amounts of earth. It has been suggested that humans have disturbed greater than one half of the terrestrial surface of Earth (Hooke et al., 2012) and that human activity – agriculture in particular – may be the largest geomorphic force on this planet (Hooke, 2000). In terms of per capita global food production, it has been argued that the role of humans as erosive agents is negligible on a global scale and over geologic time (Wilkinson and McElroy, 2007). However, a synthesis of worldwide data showed that soil erosion under conventional agriculture systems occurs at rates one to two orders of magnitude faster than rates of natural erosion and pedogenesis (Montgomery, 2007). There is clearly an imbalance between anthropogenic erosion and soil production.

Accelerated soil erosion is often harmful in two locations: where the soil particles are detached and where the sediment is deposited. Erosional landscape positions are characterized by net topsoil loss, which lowers inherent agricultural productivity by diminishing soil organic matter, lowering available water holding capacity, decreasing rooting depth, and removing natural or artificial nutrients (Cruse et al., 2013). Uncontrolled anthropogenic erosion can decrease productivity by 5% to 10% within only one century and can render some land entirely unsuitable for agriculture until pedogenesis has replaced lost topsoil (Larson et al., 1983). Research in Iowa, USA, has shown that maize yields were reduced by 10% and 23% on severely eroded soils formed

in loess and glacial till, respectively, relative to slightly eroded soils of the same series and that such reductions may necessitate higher rates of fertilizer application to maintain yields (Fenton et al., 2005), thereby increasing production costs. Soil erosion is a delicate environmental problem because it is typically part of a positive feedback of less biomass production, lowered soil organic matter, slower infiltration, and increased runoff – which promotes further soil loss (Hatfield et al., 2013). Because land is also removed from production for non-agricultural human development (Cruse et al., 2013), it is paramount that remaining agricultural land be managed in ways that limit or eliminate degradative processes such as soil erosion. Practices and structures that control soil erosion can impose financial burdens to producers, but there is also a cost to allowing soil to erode – and such costs negatively impact both producers and off-farm stakeholders (Faeth, 1993; Pimentel et al., 1995; Uri, 2000). Recognition of the economic value of soil could lead to improved conservation implementation and lesser costs externalized to non-agricultural sectors of society (Faeth, 1993; Zhou et al., 2009).

Soil erosion negatively affects ecosystems and economics beyond the area of soil removal because the ensuing deposition adds sediment and chemicals to landscape elements that naturally would not receive such a high sediment load. Soil particles can alter local hydrologic regimes by filling reservoirs or disrupting stream flow by altering bank and bed morphology. Eroded soil consists not only of mineral solids but also of dissolved and adsorbed nutrients. Such nutrients, especially phosphorus and nitrogen often sourced from anthropogenic soil amendments and fertilizers, disrupt aquatic ecosystems. Impaired water quality in upland agricultural watersheds imposes purification costs on downstream municipalities, decreases water body recreational value,

and ultimately contributes to hypoxia in terminal waters. Many of these challenges could be averted if sediment was not deposited in waterways. However, agricultural landscapes are effectively connected to streams through a specific type of soil displacement called ephemeral gully erosion.

An ephemeral gully is a temporary channel that is formed by the erosive force of concentrated overland flow. Because they tend to form in lower field reaches (Zheng et al., 2005) and easily convey runoff, ephemeral gullies increase surficial drainage network connectivity by linking uplands to streams (Gordon et al., 2008; Ohde, 2011). Ephemeral gully erosion is distinguished from sheet and rill erosion on the basis that it occurs in non-random landscape positions (swales), whereas sheet and rill erosion occur randomly and uniformly on planar hillslopes (Casalí et al., 2006). Ephemeral gully erosion lowers agricultural productivity both within gullies because crops rarely grow in channels (Cheng et al., 2006) and adjacent to topographic concavities because channels are frequently filled with nearby soil which reduces local topsoil depth beyond the gully itself (Martínez-Casasnovas et al., 2005; Gordon et al., 2008). Fill operations allow channels to redevelop due to subsequent runoff events, which has two primary consequences: soil loss via ephemeral channel erosion is perpetuated (Martínez-Casasnovas et al., 2005) and a reinforcing feedback of local steepening that leads to landscapes on which overland flow is more efficiently concentrated, thereby further increasing future risk of concentrated flow erosion (Poesen et al., 1996b). The significance of ephemeral gully erosion is well-recognized within the scientific community (e.g. Poesen et al., 2003), but there is still much to be learned about this unique phenomenon.

Substantial advances in predictive modeling of ephemeral gullies have been made (e.g. Gordon et al., 2007; Gordon et al., 2008; Wells et al., 2009; Wells et al., 2010; Gordon et al., 2012; Momm et al., 2012; Momm et al., 2013; Wells et al., 2013), and ephemeral gully erosion has been accurately simulated within the context of total (sheet, rill, channel, and tillage) field-scale erosion (Dabney et al., 2014). Such efforts are improvements over commonly used field-scale models such as the Revised Universal Soil Loss Equation 2 (RUSLE2: USDA-ARS, 2013) and the Water Erosion Prediction Project hillslope model (WEPP: Flanagan et al., 1995), which only estimate sheet and rill erosion (Flanagan et al., 1995; Bennett et al., 2000; Gordon et al., 2007; USDA-ARS, 2013). Newly developed models that explicitly account for ephemeral gully erosion must be validated with field measurements (Poesen et al., 1996a; Stroosnijder, 2005) – of which there is a dearth at the small-field or large-hillslope scale (Deasy et al., 2011). The preferred technique for measuring erosion at such scales is by quantifying changes in gully morphology (Stroosnijder, 2005). There also exists a lack of measurements made specifically of ephemeral channels over multi-year timeframes (Dabney et al., 2011).

While there exists an array of suitable methods to measure ephemeral gully evolution in agricultural fields (Castillo et al., 2012), one well-established yet still-developing and promising technique is photogrammetry, which is the science of using photographs to make measurements. Classical stereo photogrammetry has been used to quantify ephemeral gully erosion (Thomas et al., 1986) and reconstruct soil surfaces at large scales (Welch et al., 1984; Warner, 1995). Close-range digital photogrammetry has been shown to accurately reconstruct ephemeral gully morphology (Castillo et al., 2012; Nouwakpo and Huang, 2012) and has been used to assess gully development (Gómez-

Gutiérrez et al., 2014; Kaiser et al., 2014). However, there is still a lack of long-term, field-scale digital measurements of ephemeral channel evolution in multiple agricultural fields that could be utilized to validate or calibrate predictive models. Ultimately, improved models will enhance soil conservation planning.

The research presented in this thesis has employed close-range digital photogrammetry to quantify ephemeral gully erosion and generate morphological data of channel development to be used for model validation. The specific photogrammetric method was analyzed and its accuracy was quantified. The technique was applied to 12 field-scale sub-catchments in Iowa during 2013 and 2014. The results demonstrate that close-range digital photogrammetry is a valid and efficient approach to digitally reconstruct a time-series of ephemeral gully morphologies that may be used to improve predictive models and to estimate soil erosion by topographically concentrated runoff.

References

Bennett, S.J., J. Casalí, K.M. Robinson, and K.C. Kadavy. 2000. Characteristics of actively eroding ephemeral gullies in an experimental channel. Trans. ASABE 43(3):641-649.

Casalí, J., J. Loizu, M.A. Campo, L.M. De Santisteban, and J. Álvarez-Mozos. 2006. Accuracy of methods for field assessment of rill and ephemeral gully erosion. Catena 67(2):128-138.

Castillo, C., R. Pérez, M.R. James, J.N. Quinton, E.V. Taguas, and J.A. Gómez. 2012. Comparing the accuracy of several field methods for measuring gully erosion. Soil Sci. Soc. Am. J. 76(4):1319-1332.

Cruse, R., D. Abbas, K. Gesch, C. Kowaleski, U. Kreuter, K. LaValley, C. Lepczyk, H. Salwasser, V. Scott, and M. Willig. 2014. Grand challenge 1: Sustainability. In: Science, education, and outreach roadmap for natural resources. Association of Public and Land-grant Universities Board on Natural Resources and Board on Oceans, Atmosphere, and Climate, Washington DC. p. 16-27.

Cruse, R.M., S. Lee, T.E. Fenton, E. Wang, and J. Laflen. 2013. Soil renewal and sustainability. In: R. Lal and B.A. Stewart, editors, Principles of sustainable soil management in agroecosystems. CRC Press, Boca Raton, FL. p. 477-500.

Dabney, S.M., D.C. Yoder, D.A.N. Vieira, and R.L. Bingner. 2011. Enhancing RUSLE to include runoff-driven phenomena. Hydrol. Process. 25(9):1373-1390.

Dabney, S.M., D.A.N. Vieira, D.C. Yoder, E.J. Langendoen, R.R. Wells, and M.E. Ursic. 2014. Spatially distributed sheet, rill, and ephemeral gully erosion. J. Hydrol. Eng. C4014009:1-12.

Deasy, C., S.A. Baxendale, A.L. Heathwaite, G. Ridall, R. Hodgkinson, and R.E. Brazier. 2011. Advancing understanding of runoff and sediment transfers in agricultural catchments through simultaneous observations across scales. Earth Surf. Process. Landforms 36(13):1749-1760.

den Biggelaar, C., R. Lal, K. Wiebe, and V. Breneman. 2003a. The global impact of soil erosion on productivity I: Absolute and relative erosion-induced yield losses. Adv. in Agron. 81:1-48.

den Biggelaar, C., R. Lal, K. Wiebe, H. Eswaran, V. Breneman, and P. Reich. 2003b. The global impact of soil erosion on productivity II: Effects on crop yields and production over time. Adv. in Agron. 81:49-95.

Dominati, E., M. Patterson, and A. Mackay. 2010. A framework for classifying and quantifying the natural capital and ecosystem services of soils. Ecological Economics 69(9):1858-1868.

Faeth, P. 1993. Evaluating agricultural policy and the sustainability of production systems: An economic framework. J. Soil Water Conserv. 48(2):94-99.

Fenton, T.E., M. Kazemi, and M.A. Lauterbach-Barrett. 2005. Erosional impact on organic matter content and productivity of selected Iowa soils. Soil Tillage Res. 81(2):163-171.

Flanagan, D.C., J.C. Ascough II, A.D. Nicks, M.A. Nearing, and J.M. Laflen. 1995. Chapter 1: Overview of the WEPP erosion prediction model. In: USDA-Water Erosion Prediction Project hillslope profile and watershed model documentation, NSERL Report No. 10. USDA-Agricultural Research Service, West Lafayette, IN.

Gómez-Gutiérrez, Á., S. Schnabel, F. Berenguer-Sempere, F. Lavado-Contador, and J. Rubio-Delgado. 2014. Using 3D photo-reconstruction methods to estimate gully headcut erosion. Catena 120:91-101.

Gordon, L.M., S.J. Bennett, R.L. Bingner, F.D. Theurer, and C.V. Alonso. 2007. Simulating ephemeral gully erosion in AnnAGNPS. Trans. ASABE 50(3):857-866.

Gordon, L.M., S.J. Bennett, C.V. Alonso, and R.L. Bingner. 2008. Modeling long-term soil losses on agricultural fields due to ephemeral gully erosion. J. Soil Water Conserv. 63(4):173-181.

Gordon, L.M., S.J. Bennett, and R.R. Wells. 2012. Response of a soil-mantled experimental landscape to exogenic forcing. Water Resour. Res. 48:W10514.

Hatfield, J.L., R.M. Cruse, and M.D. Tomer. 2013. Convergence of agricultural intensification and climate change in the Midwestern United States: implications for soil and water conservation. Mar. Freshwater Res. 64(5):423-435.

Hatfield, J., G. Takle, R. Grotjahn, P. Holden, R.C. Izaurralde, T. Mader, E. Marshall, and D. Liverman. 2014. Chapter 6: Agriculture. In: J.M. Melillo, T.C. Richmond, andG.W. Yohe, editors, Climate change impacts in the United States: The third national climate assessment. US Global Change Research Program, Washington DC. p. 150-174.

Hillel, D. 2008. Soil in the environment: Crucible of terrestrial life. Elsevier Inc. Academic Press, Burlington, MA.

Hooke, R.L. 2000. On the history of humans as geomorphic agents. Geology 28(9):843-846.

Hooke, R.L., J.F. Martín-Duque, and J. Pedraza. 2012. Land transformation by humans: A review. GSA Today 22(12):4-10.

Jenny, H. 1941. Factors of soil formation: A system of quantitative pedology. McGraw-Hill Book Company, Inc., New York.

Johnson, D.L., and D. Watson-Stegner. 1987. Evolution model of pedogenesis. Soil Sci. 143(5):349-366.

Kaiser, A., F. Neugirg, G. Rock, C. Müller, F. Haas, J. Ries, and J. Schmidt. 2014. Small-scale surface reconstruction and volume calculation of soil erosion in complex Moroccan gully morphology using structure from motion. Remote Sens. 6(8):7050-7080.

Lal, R. 2001. Soil degradation by erosion. Land Degrad. Dev. 12(6):519-539.

Larson, W.E., F.J. Pierce, and R.H. Dowdy. 1983. The threat of soil erosion to long-term crop production. Science 219(4584):458-465.

Martínez-Casasnovas, J.A., M. Concepción Ramos, and M. Ribes-Dasi. 2005. On-site effects of concentrated flow erosion in vineyard fields: some economic implications. Catena 60(2):129-146.

Momm, H.G., R.L. Bingner, R.R. Wells, and D. Wilcox. 2012. AGNPS GIS-based tool for watershed-scale identification and mapping of cropland potential ephemeral gullies. Appl. Eng. Agric. 28(1):17-29.

Momm, H.G., R.L. Bingner, R.R. Wells, J.R. Rigby, and S.M. Dabney. 2013. Effect of topographic characteristics on compound topographic index for identification of gully channel initiation locations. Trans. ASABE 56(2):523-537.

Montgomery, D.R. 2007. Soil erosion and agricultural sustainability. Proc. Natl. Acad. Sci. 104(33):13268-13272.

Newton, I. 1729. The mathematical principles of natural philosophy (Philosphiæ naturalis principia mathematica). Translated by A. Motte. Originally published 1687.

Nouwakpo, S.K., and C. Huang. 2012. A simplified close-range photogrammetric technique for soil erosion assessment. Soil Sci. Soc. Am. J. 76(1):70-84.

Ohde, N.R. 2011. Ephemeral gullies and ecosystem services: Social and biophysical factors. MS thesis, Iowa State University.

Pimentel, D., C. Harvey, P. Resosudarmo, K. Sinclair, D. Kurz, M. McNair, S. Crist, L. Shpritz, L. Fitton, R. Saffouri, and R. Blair. 1995. Environmental and economic costs of soil erosion and conservation benefits. Science 267(5201):1117-1123.

Poesen, J.W., J. Boradman, B. Wilcox, and C. Valentin. 1996a. Water erosion monitoring and experimentation for global change studies. J. Soil Water Conserv. 51(5):386-390.

Poesen, J.W., K. Vandaele, and B. Van Wesemael. 1996b. Contribution of gully erosion to sediment production on cultivated lands and rangelands. In: Erosion and sediment yield: Global and regional perspectives, Proceedings of the Exeter Symposium, IAHS Publication No. 236. p. 251-266.

Poesen, J. J. Nachtergaele, G. Verstraeten, and C. Valentin. 2003. Gully erosion and environmental change: importance and research needs. Catena 50(2-4):91-133.

Schaetzl, R.J., and S. Anderson. 2005. Soils: Genesis and geomorphology. Cambridge University Press, Cambridge, UK.

Simonson, R.W. 1959. Outline of a generalized theory of soil genesis. Soil Sci. Soc. Am. Proc. 23(2):152-156.

Stroosnijder, L. 2005. Measurement of erosion: Is it possible? Catena 64(2-3):162-173.

Thomas, A.W., R. Welch, and T.R. Jordan. 1986. Quantifying concentrated-flow erosion on cropland with aerial photogrammetry. J. Soil Water Conserv. 41(4):249-252.

Uri, N.D. 2000. Agriculture and the environment – the problem of soil erosion. J. Sustain. Agric. 16(4):71-94.

USDA -Agricultural Research Service (USDA-ARS). 2013. Science documentation: Revised Universal Soil Loss Equation version 2 (RUSLE 2). USDA-Agricultural Research Service, Washington, DC.

Warner, W.S. 1995. Mapping a three-dimensional soil surface with hand-held 35 mm photography. Soil Tillage Res. 34(3):187-197.

Welch, R., T.R. Jordan, and A.W. Thomas. 1984. A photogrammetric technique for measuring soil erosion. J. Soil Water Conserv.n 39(3):191-194.

Wells, R.R., C.V. Alonso, and S.J. Bennett. 2009. Morphodynamics of headcut development and soil erosion in upland concentrated flows. Soil Sci. Soc. Am. J. 73(2):521-530.

Wells, R.R., S.J. Bennett, and C.V. Alonso. 2010. Modulation of headcut soil erosion in rills due to upstream sediment loads. Water Resour. Res. 46:W12531.

Wells, R.R., H.G. Momm, J.R. Rigby, S.J. Bennett, R.L. Bingner, and S.M. Dabney. 2013. An empirical investigation of gully widening rates in upland concentrated flows. Catena 101:114-121.

Wilkinson, B.H., and B.J. McElroy. 2007. The impact of humans on continental erosion and sedimentation. Geol. Soc. Am. Bull. 119(1-2):140-156.

Zheng, F., X. He, X. Gao, C. Zhang, and K. Tang. 2005. Effects of erosion patterns on nutrient loss following deforestation on the Loess Plateau of China. Agric., Ecosyst. Environ. 108(1):85-97.

Zhou, X., M.J. Helmers, M. Al-Kaisi, and H.M. Hanna. 2009. Cost-effectiveness of cost-benefit analysis of conservation management practices for sediment reduction in and Iowa agricultural watershed. J. Soil Water Conserv. 64(5):314-323.

CHAPTER 2

QUANTIFYING UNCERTAINTY OF MEASURING GULLY MORPHOLOGICAL EVOLUTION WITH CLOSE-RANGE DIGITAL PHOTOGRAMMETRY

Modified from a manuscript accepted by *Soil Science Society of America Journal*

K.R. Gesch, R.R. Wells, R.M. Cruse, H.G. Momm, and S.M. Dabney

Abstract

Measurement of geomorphic change may be of interest to researchers and practitioners in a variety of fields including geology, geomorphology, hydrology, engineering, and soil science. Landscapes are often represented by digital elevation models. Surface models generated of the same landscape over a time interval can be compared to estimate geomorphic evolution. Any such morphological estimate of change in a landform should include a range of probable values based on the quality of the digital elevation models that represent the surface of interest. This study sought to determine the uncertainty associated with detecting changes in reaches of ephemeral gullies with close-range digital photogrammetry. An experimental surface was constructed, surveyed, and photographed. The images were used as input to photogrammetry software to generate point clouds, which were then analyzed to determine the quality of elevation data generated by the photogrammetric technique. For individual point clouds the 2σ relative vertical accuracy was determined to equal 0.916 mm and the 2σ absolute (geo-referenced) vertical accuracy was computed as 8.26 cm, and the 95% confidence range (2σ uncertainty) of detecting elevation change between two point clouds was determined to be ± 1.29 to ± 2.55 mm, depending on relief. These values could be applied to volumetrically derived estimates of geomorphic change as an uncertainty range. The high vertical accuracy and small uncertainty in elevation change determined in this study

suggest that close-range digital photogrammetry is an effective and acceptable method to accurately detect small changes in ephemeral gullies or other geomorphic features of interest.

Introduction

Characterizing morphological evolution of ephemeral gullies and rills in agricultural landscapes with traditional surveying methods is often limited by the dynamic nature and small size of such channels. Photogrammetry constitutes a viable alternative for the digital reconstruction and measurement of micromorphological landscape elements. Photogrammetry is defined as the science of deriving three-dimensional measurements and models of an object from two or more two-dimensional photographs of that object and its surroundings (Mikhail et al., 2001; Kasser and Egels, 2002; Luhmann et al., 2006).

The first step of digital photogrammetry is resection, which utilizes known camera lens properties to locate the center of each camera sensor in three-dimensional image space (Mikhail et al., 2001). Next, the accurate location and orientation (pose) of each camera sensor are used as input for image matching, which is performed by specialized algorithms that locate conjugate points in a stereo set of digital images and calculate their three-dimensional coordinates (Schenk, 1996). When generating a continuous digital representation of topography, such as a digital elevation model (DEM), the set of matched points is converted into a three-dimensional surface by interpolation (Schenk, 1996). Both the pixel matching and the interpolation processes can introduce error into the final DEM, where such error represents the discrepancy between the DEM and the actual surface that it models. DEM error is typically constrained to the spatial

domain because photogrammetric surface reconstruction yields a DEM that corresponds to the surface at the unique time of image acquisition.

Repeated photogrammetric surveys of experimental and natural landforms can be used to detect and assess geomorphic change (e.g. Welch et al., 1984; Stojic et al., 1998; Brasington and Smart, 2003; James and Robson, 2012). Aerial photogrammetry has been used to study fluvial and upland channel erosion processes including stream evolution (Lane et al., 2003; Fonstad et al., 2013) and classical and ephemeral gully erosion (Thomas et al., 1986; Nachtergaele and Poesen, 1999; Marzolff and Poesen, 2009). However, the large object distance (measured from camera to land surface) on the order of 10^1 to 10^2 m utilized in aerial photogrammetry limits the spatial resolution of any DEM that is generated to represent the geomorphic feature of interest. Ground resolution is constrained by pixel size because a pixel is the basic unit for image matching procedures. High camera altitude corresponds to a small pixel-to-ground ratio and thus a low maximum horizontal resolution. Conversely, in images obtained at low altitudes each pixel represents a much smaller area in object space and therefore the potential DEM resolution is larger. Thus, closer cameras capture more detail (James and Robson, 2012; Fonstad et al., 2013). Vertical accuracy is also constrained by object distance (Ackermann, 1996).

Close-range photogrammetry (i.e. object distance < 10 m) has been manually implemented to reconstruct soil surfaces at improved horizontal resolution (10^{-1} to 10^{-2} m or higher) and vertical accuracy (10^{-2} to 10^{-3} m), which are necessary for soil erosion research (Welch et al., 1984; Warner, 1995). More recently, digital close-range photogrammetry has been shown to outperform manual photogrammetry (Hancock and

Willgoose, 2001) and to compare favorably with terrestrial laser scanning (Aguilar et al., 2009; Castillo et al., 2012; James and Robson, 2012; Nouwakpo and Huang, 2012) with respect to the quality of derived topographic data. Due to its capacity to generate high-resolution data, photogrammetry has been applied to the study of soil erosion and drainage network evolution in laboratory and runoff plot environments (Rieke-Zapp and Nearing, 2005; Gessesse et al., 2010; Heng et al., 2010; Gordon et al., 2012). Close-range photogrammetry has been used to produce single time step DEMs of gullies in agricultural landscapes (Castillo et al., 2012; Nouwakpo and Huang, 2012) and to monitor headcut development (Gómez-Gutiérrez et al., 2014; Kaiser et al., 2014). DEMs of entire channels obtained sequentially over longer timeframes would allow for multi-temporal surface comparison and determination of long-term morphometric sediment flux as a proxy measurement of geomorphic evolution.

A field study was designed to utilize time-sequenced photogrammetry to generate a collection of topographic data of reaches of ephemeral channels (Wells et al., in prep.). The dataset was used to derive estimates of morphological change within monitored reaches of ephemeral gullies by determining volume change between multiple dates. Computed morphological change (i.e. channel evolution) is not without error and ultimately is tied to DEM quality (Heritage et al., 2009). Erosion- and deposition-induced volumetric changes must account for uncertainties associated with the source of topographic data (Lane et al., 2003; Heng et al., 2010), which in this study was close-range digital photogrammetry.

The study initiated by Wells et al. (in prep.) focused on development of a specific method of data collection via photogrammetry, a scheme for post-processing the

photogrammetric data, and an experimental setup to apply the specific photogrammetric method in a field setting. This study sought to evaluate the method (this chapter) and to apply it in agricultural fields (Chapter 3).

In this research, photogrammetry was used to generate raw point clouds of ephemeral gully reaches (Wells et al., in prep.). A point cloud is a collection of irregularly distributed points that each contain a three-dimensional location recorded in a (X, Y, Z) tuple. A raw point cloud can then be used to generate a DEM as a regularly spaced raster grid. Automated point cloud extraction or DEM generation from photographs are specific instances of surface reconstruction, which is a mathematically ill-posed problem because its solution may not exist nor is that solution necessarily unique and robust (Schenk, 1996; Paparoditis and Dissard, 2002). Because a DEM is an imperfect surface representation, it follows that any measurement obtained from a DEM must deviate from the corresponding true (yet theoretically unobtainable) value. Likewise, the photogrammetric measurement technique also contains errors that should be quantified, which was the purpose for this study. The reliability of topographic analyses and topographically derived parameters are limited by the errors inherent in the DEM used (Abd Aziz et al., 2012; Momm et al., 2013). Furthermore, when DEMs of the same surface are generated at multiple time steps, errors in the individual DEMs are propagated into any calculations of volumetric change over that time interval (Brasington et al., 2000; Fuller et al., 2003; Lane et al., 2003; Wheaton et al., 2010). One goal of the research program is to utilize sequential DEMs to determine volumetric change within reaches of ephemeral gullies due to precipitation and runoff events (Wells et al., in prep.), so accounting for DEM uncertainty is critical.

Because errors in DEMs influence the detection of morphological evolution, the volume change calculations for field-monitored channel reaches may misrepresent actual erosional or depositional change. To rectify this, two procedures were used to determine the uncertainties embedded in this application of close-range digital photogrammetry. The objective of this study was to use the results of these analyses to define the uncertainty associated with morphometric estimates of landform change and the relative and absolute vertical accuracy of geospatial data generated with close-range photogrammetry.

Methods

To quantify the intrinsic methodological uncertainty, two analyses were conducted. First, the error due to DEM differencing was determined. Second, the relative and absolute vertical errors of point clouds generated with close-range digital photogrammetry were established. Both analyses were performed using point clouds generated from photographs of the same experimental setup.

A simulated channel reach was established on a flat asphalt surface. This reach was intended to mimic the design of in-field ephemeral gully reaches. The reach was defined as the area within a 1.8 m by 1.2 m PVC frame, which was also utilized for the placement of anchor points that delineated channel reaches monitored in the field study (Wells et al., in prep.). Asphalt was chosen as the experimental surface because it was primarily flat and smooth yet still had modest texture on a gentle slope. Within the reach, 35 photogrammetric targets were placed in a 0.3 m grid (Figure 1). The targets were surveyed with a Trimble R8 real-time kinematic global positioning system (RTK-GPS) receiver, which has maximum horizontal and vertical accuracies of 0.8 cm and 1.5 cm,

respectively (Trimble Navigation Ltd., 2013). The receiver was connected to the Iowa Real-Time Network (IaRTN) maintained by the Iowa Department of Transportation, which is a network of base stations with a 1σ vertical accuracy of 2 to 3 cm (Iowa DOT, 2014). This RTK-GPS survey dataset was used as the reference dataset in the subsequent analyses. Of the 35 targets, the four that were located in the reach corners were used as ground control points (GCPs) for photogrammetric processing and the 31 remaining targets were used as validation points (VPs). The GCPs in this configuration correspond to field reaches defined by sets of four surveyed reference stakes placed sequentially along actual channels. The GCPs were used as vertices of a quadrilateral that defined the extents of the asphalt reach, which had an area of 2.11 m^2.

The experimental reach was photographed with a non-metric pre-calibrated Nikon D7000 digital single-lens reflex camera containing an AF Nikkor lens with f/2.8D aperture and fixed 20 mm focal length. Image files were saved in JPEG format. The camera was mounted on a metal frame attached to a backpack. The photographer then wore the backpack which resulted in a camera height of approximately 3.1 m. The camera was connected to a Cam Ranger wireless router that allowed the photographer to use an iPad to view the imaging area and capture photographs without touching the camera (Wells et al., in prep.).

Two sequences of convergent oblique images were obtained, and every photograph contained the entire reach. When oblique camera angles are used the size of a pixel in object space is dependent upon its location in image space (Heng at al., 2010), so camera location must be known or solvable. In this case, camera locations were automatically determined during photogrammetric processing using the camera

calibration parameters. Oblique photographs were used because images that converge on the scene improve the solution of camera orientation and thus also the accuracy of the reconstructed surface (Stojic et al., 1998; Eos Systems Inc., 2012). First, eight photographs were taken in a circular fashion around the reach. Automatically resolved camera positions for the first sequence of images are shown in Figure 2. In field-based photography of channel reaches, one photograph is obtained from the downstream side facing upstream parallel to the channel and a second is taken from the upstream side of the reach facing downstream (Wells et al., in prep.). To mimic this procedure the second set of photographs included three images from the "downstream" side and three images from the "upstream" side of the experimental reach.

The eight photographs obtained in the first sequence were all used as input to generate a point cloud in PhotoModeler Scanner (Eos Systems Inc., 2014). To create the point cloud, first all eight images were matched with PhotoModeler Scanner's automated image matching procedure, which is based on the scale-invariant feature transform (SIFT) algorithm (Lowe, 2004). The four GCPs in every photograph were each manually identified and then cross-referenced to the corresponding GCP in each of the other images. The GCPs were then geo-referenced using the RTK-GPS survey data. Geo-referencing prior to point cloud generation is beneficial because it automatically scales and orients the point cloud as it is computed. Finally, the point cloud was generated using the Create Dense Surface command within PhotoModeler Scanner. All paired photos were used, sampling interval was set to 5 mm, and default meshing options were used. The resulting point cloud was exported as a text file (Figure 3).

The set of six additional photographs was used to generate nine point clouds with PhotoModeler Scanner. Each of the "upstream" facing photographs was matched with each of the "downstream" facing photographs for a total of nine image pairs. Every image pair was used as input to create a point cloud according to the procedure described above, with the only difference being that two photographs were used instead of eight. The image pairs and corresponding point clouds are shown in Figure 4. The resulting nine point clouds were exported as text files.

Comparison of replicated models of the same surface has been proposed (Heng et al., 2010; Wheaton et al., 2010) and used (Brasington and Smart, 2003) as an approach to assess DEM uncertainty. This tactic was adopted for the ensuing analysis. Each of the nine point clouds generated from the second image set was paired with every other point cloud for a total of 36 pairs. Wells et al. (in prep.) have developed a straightforward procedure that can be applied to determine the discrepancy, expressed as volumetric change, between the surfaces approximated by two point clouds. This is mathematically analogous to subtracting one surface from the other. In theory, any volume difference thus computed using the 36 point cloud pairs should equal 0 m^3 because the nine point clouds represent the same surface. However, the errors inherent in any general case of surface reconstruction and in this specific application of close-range photogrammetry suggest that the inevitable inconsistencies between point clouds should result in a non-zero volume difference.

To verify this supposition, volumetric discrepancy, ΔV, between surfaces was calculated for all 36 point cloud pairs using the point cloud post-processing approach of Wells et al. (in prep.), which is briefly summarized here. Two input point cloud files *p*

and q are interpolated to a 5 mm raster grid containing $i \times j$ cells, each with elevation Z_{ij}. The volume difference between the surfaces represented by p and q is given by

$$\Delta V = a \sum_{i} \sum_{j} \left(Z_q - Z_p \right) \tag{1}$$

where a is the area of one raster cell (equal for all cells), i and j are indices corresponding to the location of an individual cell, and Z_p and Z_q are the interpolated elevations at cell ij within the DEMs fitted from p and q, respectively.

When subtracting the replicate surfaces approximated by the nine point clouds, the minuend and subtrahend were determined with a random number generator. For each point cloud pair a 0 dictated that the point cloud represented by the alphabetically later letter would serve as the minuend (e.g. $\Delta V_{AB} = B - A$); a 1 indicated the opposite (e.g. $\Delta V_{AB} = A - B$). The distribution of volumetric changes was assessed and summary statistics were calculated using R statistical software (R Core Team, 2013). Two times the standard deviation (2σ) of the population of volume changes was taken as the uncertainty in calculation of volume change, $\delta\Delta V$, as determined by the photogrammetric method employed in this study, where two standard deviations of a population with a Gaussian distribution approximates a 95% confidence level (Taylor, 1997). Normality of all populations was verified with the Shapiro-Wilk test.

The quality of the elevation information contained in the point clouds was then assessed. For all nine point clouds the elevation of each of the 31 VPs was compared with the elevation of the closest point in the point cloud, which was determined with an in-house Python script. Raw point clouds rather than rasterized DEMs were used as input to preclude any interpolation errors. The program utilizes the NumPy library (Dubois et al., 1996; van der Walt et al., 2011) to rapidly organize and query point cloud geospatial data

for the nearest neighbor of every validation point. Once the nearest neighbor is located, the distance between the VP currently under consideration and its nearest neighbor along with the elevation difference between them are computed and recorded. Elevation difference, $\hat{Z}$, is calculated by

$$\hat{Z} = Z_{NN} - Z_{VP} \tag{2}$$

where Z_{NN} is the elevation value of the nearest neighbor within the point cloud and Z_{VP} is the elevation of the validation point against which the neighbor is being compared. The formulation of Equation 2 suggests that for any validation point VP_i if the corresponding elevation difference $\hat{Z}_i > 0$ then the surface approximated by the point cloud overestimates elevation relative to the surveyed VP_i, which serves as the reference value. The inputs, processes, and outputs of the nearest neighbor search-and-compare algorithm are summarized in Figure 5. The results of running the script with nine point clouds and 31 VPs were outputted as a text file and analyzed with R statistical software.

In determination of photogrammetric point cloud quality, the spatially averaged elevation difference was used to compute the relative vertical accuracy, δZ_{rel}, and the standard deviation of validation point-to-nearest neighbor elevation differences was understood to represent the absolute (geo-referenced) vertical accuracy, $\delta Z_{\text{geo-ref}}$, of the point clouds. Uncertainty of elevation change, $\delta\Delta Z$, was defined as

$$\delta\Delta Z = \delta\Delta V / A_R \tag{3}$$

where A_R is the area of the reach. This is analogous to average volume change per unit area, or mean elevation difference across an entire surface model. Vertical change uncertainty was derived from volumetric change uncertainty because determination of volumetric change within channel reaches is one goal of the field study. Furthermore,

utilization of descriptive statistics from a population of volume differences to define the probable range of vertical change accounts for additional errors that may be introduced by interpolation and rasterization during point cloud post-processing. The use of volume change uncertainty to establish elevation change uncertainty is based on the assumption that vertical uncertainty is not spatially variable within the reach, that is for any individual point cloud the error associated with elevation is uniform at all locations within that point cloud. The value calculated by Equation 3 is associated with uncertainty of change in elevation between DEMs. This value is actually a combination of the vertical uncertainty of each surface in a pair. If the vertical errors of individual DEMs *p* and *q* are assumed to be independent and random, then they can be propagated into vertical change error, $\varepsilon_{\Delta Z}$, using the sum in quadrature approach of Taylor (1997, Equation 3.16) such that

$$\varepsilon_{\Delta Z} = \sqrt{\left(\delta Z_p\right)^2 + \left(\delta Z_q\right)^2} \tag{4}$$

where δZ_p and δZ_q are the vertical uncertainties associated with the surfaces approximated by point clouds *p* and *q*, respectively, and $\varepsilon_{\Delta Z}$is equivalent to $\delta\Delta Z$. If it is assumed that the vertical uncertainties of individual surfaces *p* and *q* are equal such that $\delta Z_p = \delta Z_q = \delta Z_{\text{rel}}$ then Equation 4 can be rearranged and simplified to yield

$$\delta Z_{\text{rel}} = 0.707\varepsilon_{\Delta Z} \tag{5}$$

where δZ_{rel} is the vertical uncertainty of the surface described by any one point cloud. This value is useful as an indicator of vertical accuracy because it provides a measure of typical elevation discrepancy across the entire horizontal area described by a point cloud. Similarly, the volume change calculation in Equation 1 integrates elevation change over the entire raster grid area.

Two times the sample standard deviation (2σ), root mean square error (RMSE), and mean absolute error (MAE), were calculated as metrics of uncertainty for ΔV, $\delta\Delta Z$, δZ_{rel}, and $\delta Z_{\text{geo-ref}}$ with the following equations:

$$2\sigma = 2\sqrt{\frac{1}{N-1}\sum(\varepsilon_i - \bar{\varepsilon})^2} \tag{6}$$

$$\text{RMSE} = \sqrt{\frac{1}{N}\sum {\varepsilon_i}^2} \tag{7}$$

$$\text{MAE} = \frac{1}{N}\sum|\varepsilon_i| \tag{8}$$

where N is a sample size; ε_i is an individual error of volume change, elevation change, or elevation; and $\bar{\varepsilon}$ is the mean error of an entire population of volume change, elevation change or elevation errors.

Results

The point cloud generated with the set of eight photographs contained 2,468,517 points within the reach area of 2.11 m^2, which corresponded to a point density of 1.17 points mm^{-2}. Point clouds *A* through *I* generated from the set of six images contained an average of 94,620 points inside the reach, or 0.045 points mm^{-2}.

A histogram of the 36 computed volume differences is shown in Figure 6, and a Shapiro-Wilk test ($W = 0.986$, $p = 0.9195$) validated the graphical evidence of a Gaussian distribution. Mean volume difference was 2.06×10^{-4} m^3 and the sample standard deviation of volume differences was 1.37×10^{-3} m^3. Thus $\delta\Delta V$ within the experimental reach was defined as $\pm 2.73 \times 10^{-3}$ m^3. A one-sample *t*-test ($t = 0.9047$, df = 35, $p = 0.3718$) showed that the mean volumetric discrepancy was not significantly different

from zero. Based on this value of $\delta\Delta V$, the 2σ uncertainty of elevation change, $\delta\Delta Z$, was calculated as ± 1.29 mm with Equation 3. Inserting this value into Equation 5 yielded an individual point cloud 2σ relative vertical uncertainty, δZ_{rel}, of 0.916 mm. Figure 7 illustrates the distribution of spatially averaged elevation discrepancies (computed by dividing the population of volume differences by the reach area, as in Equation 3) which had an unbiased mean of 0.098 mm (one-sample *t*-test: $t = 0.9047$, df = 35, $p = 0.3718$) and a standard deviation of 0.647 mm with a normal distribution (Shapiro-Wilk test: $W = 0.986$, $p = 0.9195$).

The results of the point cloud quality assessment via the nearest neighbor script are summarized in Figure 8. There was no significant correlation ($r = 0.245$) between validation point-to-nearest neighbor distance and elevation difference (Figure 9). Mean distance between validation points and their nearest neighbor was 3.09 mm (less than the width of one raster cell, 5 mm) and mean elevation difference was 0.465 mm, while the standard deviation of elevation differences was 4.13 cm. A Shapiro-Wilk test ($W = 0.9681$, $p = 7.274 \times 10^{-6}$) revealed that the population of elevation differences did not have a Gaussian distribution. Based on a one-sample *t*-test ($t = 0.188$, df = 278, $p = 0.851$), the mean elevation discrepancy of 0.465 mm was not statistically different from zero. Two times the standard deviation of elevation differences, 8.26 cm, was used as the 2σ geo-referenced absolute vertical accuracy, $\delta Z_{geo\text{-}ref}$, of photogrammetric point clouds. Together with graphical evidence of normality (Figure 8), a non-parametric 95% confidence interval of –7.39 to 11.06 cm suggests that the population of elevation differences is only approximately Gaussian because it is more heavily tailed and slightly positively skewed.

2σ values were assumed to be the preferred uncertainty metric due to the associated high level of confidence, although root mean square (RMS) error and MAE were also computed using Equations 6, 7, and 8, respectively, for $\delta\Delta Z$, δZ_{rel}, and $\delta Z_{geo\text{-}ref}$. These results are compiled in Table 1.

Discussion

The point cloud generated using eight images contained approximately 26 times more points than the point clouds generated using paired photographs. While the point density of 0.045 points mm^{-2} of the two-image point clouds appears to be low, it is worth noting that, during post-processing, point clouds are interpolated to 5 mm grids, which means that a 0.045 points mm^{-2} density corresponds to 1.12 points per raster cell (25 mm^2). This value suggests that interpolation-induced error should be small even when only two photographs are used because the number of points exceeds the number of raster cells. Such data redundancy typically increases DEM accuracy (Ackermann, 1996).

Because more photographs improve the accuracy of any photogrammetrically reconstructed surface (Eos Systems Inc., 2012; Fonstad et al., 2013), the validity of using only two images in lieu of eight was assessed by comparing point clouds *A* through *I* with the eight-image point cloud. The average ΔV was 2.77×10^{-3} m^3 and the corresponding average vertical difference was 1.31 mm. Both of these values compare well with the $\delta\Delta V$ and $\delta\Delta Z$ values of $\pm 2.73 \times 10^{-3}$ m^3 and ± 1.29 mm, respectively, as calculated above. The primary benefit of using only two photographs is reduced time to generate a point cloud. Using the set of eight photographs as input in PhotoModeler Scanner, an experienced operator took almost two hours to create the final point cloud, including manual GCP identification and cross-referencing in addition to automated image

matching and dense surface calculation. The same operator was able to use the exact same procedure to create point clouds in approximately 15 minutes when using only pairs of images. Because the typical volumetric and vertical differences between the surface constructed from eight photographs and surfaces from photograph pairs were similar to the 95% probability intervals for both volume change and elevation change, the time-saving approach of using only two images per point cloud was accepted on the basis that image pairs can be used to reconstruct any experimental surface of interest with sufficient accuracy.

The uncertainty associated with volume change, $\delta\Delta V$, in the experimental reach was established as $\pm 2.73 \times 10^{-3}$ m^3 based on 2σ of the population of ΔV values, which corresponds to a 95% confidence level that true volume change values are within this range from observed values. There is no significant bias to this approach, as indicated by the fact that the mean ΔV of 2.06×10^{-4} m^3 was not significantly different from zero. However, applying this volume change uncertainty to in-field ephemeral gully reaches is complicated by the fact that not every reach encompasses the exact same ground area. Thus, an uncertainty of volume change averaged per unit area, expressed as a range for elevation change (at 95% probability), is preferable. The uncertainty of vertical change, $\delta\Delta Z$, calculated as ± 1.29 mm implies a 95% probability that the discrepancy between any observed elevation change and the actual elevation change is within this amount from calculated values.

Using the $\delta\Delta Z$ value of ± 1.29 mm along with Equations 4 and 5 resulted in a 2σ relative vertical point cloud accuracy, δZ_{rel}, of 0.916 mm. The calculation of this accuracy value assumes that errors in one point cloud are independent of errors in another point

cloud. Even though some comparisons involved point clouds with a common photo (e.g. point clouds *E* and *H* both used photograph KGA_0785 for photogrammetric image processing) the fact that every point cloud had at least one unique source photograph each time it was compared with other point clouds satisfied this assumption because image matching (i.e. the SIFT algorithm) depends on both photographs in a stereo pair. This value is twice as large as the elevation standard deviation (1σ) of any one point cloud relative either to itself or to another point cloud that exists in the same arbitrary (i.e. not geo-referenced) Euclidian three-dimensional space of real-world scale. The theoretically obtainable vertical accuracy of a DEM can be 1×10^{-4} of the object distance (Ackermann, 1996). Thus for a camera height of approximately 3.1 m a maximum vertical accuracy of 0.31 mm could be expected. Encouragingly, the 2σ vertical point cloud uncertainty, δZ_{rel}, of 0.916 mm approaches this theoretical optimum and is on the same order of magnitude. For a reconstructed surface model of this size, a maximum vertical RMS error of 1.664 mm can be expected (Eos Systems Inc., 2012). The δZ_{rel} value of 0.916 mm is within this upper limit, as is the RMS error of an individual point cloud of 0.457 mm.

The 2σ absolute vertical accuracy, $\delta Z_{\text{geo-ref}}$, of photogrammetric point clouds as determined by comparison of validation points with their nearest neighbors was found to be 8.26 cm. This accuracy of elevation values is in an absolute sense, that is, the elevation of a point cloud with respect to a fixed vertical datum (mean sea level: the same datum of the RTK-GPS survey). Thus, there is 95% confidence that a geo-referenced point cloud – which is necessary for multi-temporal surface differencing of field-monitored channel reaches – generated by this technique is located within 8.26 cm of its true vertical location on the surface of the earth. Furthermore, the fact that the mean elevation

difference of 0.465 mm determined from the output of the nearest neighbor search-and-compare script is not significantly different from zero suggests that there is no positive or negative bias of mean point cloud elevation in real-world coordinates.

The GCPs used for geo-referencing during point cloud generation were surveyed along with the 31 validation points used to define absolute vertical accuracy. Therefore, as long as point cloud relative elevation accuracy is high (e.g. < 1 mm, as in this instance), it is logical that the absolute vertical uncertainty of any geo-referenced point cloud approaches the vertical accuracy of the survey equipment used. The $2\sigma\ \delta Z_{\text{geo-ref}}$ value of 8.26 cm is comparable to the Trimble R8 receiver and IaRTN 2σ vertical accuracy of approximately 4 to 6 cm. Optimum RTK-GPS accuracy was deemed plausible because the horizontal accuracy of the surveyed GCPs was better than 2 cm: the distances between surveyed GCP coordinates were within approximately 2 cm of the actual ground distances between GCPs on the experimental surface. RMS error is another common metric of vertical accuracy. The RMS error of the 279 validation point-to-nearest neighbor elevation differences was 4.12 cm, which also compares well with the vertical accuracy of the RTK-GPS system utilized. Thus, the accuracy of the survey equipment constrained the accuracy of geo-referenced point clouds generated with this photogrammetric approach.

Erroneous GCP information due to survey error could influence point cloud elevation. The effect of GCP measurement error on point clouds was quantified by re-generating point clouds *A* through *I* with altered GCP values, such that the GCP elevations were first increased by 10 cm and then decreased by 5 cm relative to the original survey data. It was assumed for this analysis that elevation error would be equal

for all GCPs. Each erroneous point cloud was compared to its original counterpart, which resulted in average elevation differences of 9.99 cm and –4.98 cm for the +10 cm and –5 cm cases, respectively. Thus, vertical error in GCP measurement directly impacts the elevation of all points within a point cloud.

Utilizing geo-referenced GCPs to scale and orient point clouds would not impact multi-temporal elevation change error $\delta\Delta Z$, provided that the same GCP coordinates are used to scale and orient each point cloud. However, if GCPs are re-surveyed between photography, any comparison of the resulting point clouds (based on different GCP surveys) must take into account the individual accuracies of each GCP survey. Therefore, it is recommended that GCPs be (re-)surveyed according to best practices and under optimum conditions so as to maximize their accuracy, thereby minimizing the potential error of comparing multi-temporal geo-referenced point clouds.

Choice of uncertainty metric depends on planned data use. As Table 1 indicates, there are clear differences between 2σ, RMS error, and MAE as indices of vertical geospatial data quality, such that 2σ uncertainty is the largest (i.e. the most conservative). Because no significant positive or negative vertical biases were observed, RMS error was nearly equivalent to 1σ for $\delta\Delta Z$, δZ_{rel}, and $\delta Z_{\text{geo-ref}}$. If elevation change uncertainty $\delta\Delta Z$ is used as a probability interval along with volumetric estimates of morphological development, MAE would result in the smallest range and 2σ in the largest. If vertical change uncertainty is used as a minimum detection threshold (e.g. Brasington et al., 2000; Brasington and Smart, 2003; Fuller et al., 2003; Lane et al., 2003; Heritage et al., 2009; Gessesse et al., 2010; Wheaton et al., 2010; Hugenholtz et al., 2013), choice of 2σ

would cause the most information loss whereas selection of RMS error or MAE as the threshold level of detectable geomorphic change would preserve more information.

Comparison of models generated from repeated topographic reconstructions of the same surface was utilized to establish DEM vertical uncertainty (Brasington and Smart, 2003; Heng et al., 2010; Wheaton et al., 2010) and comparison of geo-referenced point clouds against surveyed validation points was used to determine absolute accuracy of elevation data (similar to Fonstad et al., 2013). It is beneficial to use surface differencing to define uncertainty both of elevation and of vertical change because doing so accounts for all sources of potential error (e.g. interpolation and rasterization) and not solely error induced during point cloud generation. The high δZ_{rel} of 0.916 mm would allow for accurate determination of three-dimensional parameters such as soil surface roughness and four-dimensional values such as volume change, whereas the $\delta Z_{geo\text{-}ref}$ of geo-referenced point clouds of 8.26 cm would allow for confident integration of point cloud geospatial data into pre-existing DEMs with lower elevation accuracy, such as those derived from aerial laser scanning or other remote sensing techniques.

For field application of this technique to study soil erosion, it is necessary that the average magnitude of observed elevation changes be larger than the vertical change uncertainty of ± 1.29 mm. However, this $\delta\Delta Z$ value was determined using a surface with little relief (17 cm), whereas gullies have greater relief. The influence of relief on vertical change uncertainty was quantified by replicating the procedure used for the asphalt surface but with images of an actual gully reach. The reach encompassed an area of 2.16 m^2 and had relief of 63 cm. Six photographs and four surveyed GCPs were used to generate nine point clouds, which were all compared to calculate the uncertainty in

average elevation change. The 2σ uncertainty of vertical change based on post-processing of the nine point clouds with 63 cm relief was determined to equal ± 2.55 mm. The vertical change uncertainty was larger for the point clouds that represented the gully reach, but the uncertainty increase (by a factor of 1.97) was less than the relief increase (by a factor of 3.71). Therefore, depending on relief, the uncertainty of elevation change ranges from ± 1.29 to ± 2.55 mm, and uncertainty may increase further when images of deeper channels are used. A pair of convergent oblique images that both contain an entire reach and its four surveyed GCPs is all that is necessary to accurately reconstruct a segment of a channel formed by concentrated overland flow. Applying the uncertainty of elevation change (volume change per unit area, $\delta\Delta Z$) to field-monitored channels would allow for a 95% estimate confidence interval to be reported along with morphometrically derived estimates of ephemeral gully erosion.

Conclusions

Statistical analysis of the results of comparing repeated topographic models of an experimental asphalt surface yielded an individual digital elevation model 2σ relative vertical accuracy of 0.916 mm and a 2σ uncertainty of detecting elevation change between two point clouds of ± 1.29 mm. Comparison of the replicate digital surface models with a set of surveyed validation points showed that geo-referenced point clouds created with this application of close-range photogrammetry had an unbiased 2σ absolute vertical accuracy of 8.26 cm. Close-range digital photogrammetry allowed for highly accurate reconstruction of the experimental surface. The relief-dependent vertical change uncertainty range of ± 1.29 to ± 2.55 mm may be extended to estimates of channel

erosion that are based on morphological change in reaches reconstructed with close-range photogrammetry.

References

Abd Aziz, S., B.L. Steward, A. Kaleita, and M. Karkee. 2012. Assessing the effects of DEM uncertainty on erosion rate estimation in an agricultural field. Trans. ASABE 55(3):785-798.

Ackermann, F. 1996. Techniques and strategies for DEM generation. In: C.W. Greve, editor, Digitial photogrammetry: An addendum to the manual of photogrammetry. American Society of Photogrammetry and Remote Sensing, Bethesda, MD. p. 135-141.

Aguilar, M.A., F.J. Aguilar, and J. Negreiros. 2009. Off-the-shelf laser scanning and close-range digital photogrammetry for measuring agricultural soils microrelief. Biosyst. Eng. 103(4):504-517.

Brasington, J., B.T. Rumsby, and R.A. McVey. 2000. Monitoring and modelling morphological change in a braided gravel-bed river using high resolution GPS-based survey. Earth Surf. Process. Landforms 25(9):973-990.

Brasington, J., and R.M.A. Smart. 2003. Close range digital photogrammetric analysis of experimental drainage basin evolution. Earth Surf. Process. Landforms 28(3):231-247.

Castillo, C., R. Pérez, M.R. James, J.N. Quinton, E.V. Taguas, and J.A. Gómez. 2012. Comparing the accuracy of several field methods for measuring gully erosion. Soil Sci. Soc. Am. J. 76(4):1319-1332.

Dubois, P.F., K. Hinsen, and J. Hugunin. 1996. Numerical Python. Comput. Phys. 10(3):262-267.

Eos Systems Inc. 2012. Quantifying the accuracy of dense surface modeling within PhotoModeler Scanner. www.photomodeler.com/applications/documents/DSMAccuracy2012.pdf (accessed 26 July 2014).

Eos Systems Inc. 2014. PhotoModeler Scanner (64-bit). Eos Systems Inc., Vancouver, British Columbia.

Fonstad, M.A., J.T. Dietrich, B.C. Courville, J.L. Jensen, and P.E. Carbonneau. 2013. Topographic structure from motion: a new development in photogrammetric measurement. Earth Surf. Process. Landforms 38(4):421-430.

Fuller, I.C., A.R.G. Large, M.E. Charlton, G.L. Heritage, and D.J. Milan. 2003. Reach-scale sediment transfers: An evaluation of two morphological budgeting approaches. Earth Surf. Process. Landforms 28(8):889-903.

Gessesse, G.D., H. Fuchs, R. Mansberger, A. Klik, and D.H. Rieke-Zapp. 2010. Assessment of erosion, deposition and rill development on irregular soil surfaces using close range digital photogrammetry. Photogramm. Rec. 25(131):299-318.

Gómez-Gutiérrez, A., S. Schnabel, F. Berenguer-Sempere, F. Lavado-Contador, and J. Rubio-Delgado. 2014. Using 3D photo-reconstruction methods to estimate gully headcut erosion. Catena 120:91-101.

Gordon, L.M., S.J. Bennett, and R.R. Wells. 2012. Response of a soil-mantled experimental landscape to exogenic forcing. Water Resour. Res. 48:W10514. doi:10.1029/2012WR012283

Hancock, G., and G. Willgoose. 2001. The production of digital elevation models for experimental model landscapes. Earth Surf. Process. Landforms 26(5):475-490.

Heng, B.C.P., J.H. Chandler, and A. Armstrong. 2010. Applying close range digital photogrammetry in soil erosion studies. Photogramm. Rec. 25(131):240-265.

Heritage, G.L., D.J. Milan, A.R.G. Large, and I.C. Fuller. 2009. Influence of survey strategy and interpolation model on DEM quality. Geomorphology 112(3-4):334-344.

Hugenholtz, C.H., K. Whitehead, O.W. Brown, T.E. Barchyn, B.J. Moorman, A. LeClair, K. Riddell, and T. Hamilton. 2013. Geomorphological mapping with a small unmanned aircraft system (sUAS): Feature detection and accuracy assessment of a photogrammetrically-derived digital terrain model. Geomorphology 194:16-24.

Iowa Department of Transportation (Iowa DOT). 2014. Iowa Real-Time Network: Frequently asked questions. http://www.iowadot.gov/rtn/faq.html (accessed 13 August 2014).

James, M.R., and S. Robson. 2012. Straightforward reconstruction of 3D surfaces and topography with a camera: Accuracy and geoscience application. J. Geophys. Res. 117:F03017. doi:10.1029/2011JF002289

Kaiser, A., F. Neugirg, G. Rock, C. Müller, F. Haas, J. Ries, and J. Schmidt. 2014. Small-scale surface reconstruction and volume calculation of soil erosion in complex Moroccan gully morphology using structure from motion. Remote Sens. 6(8):7050-7080. doi:10.3390/rs6087050

Kasser, M., and Y. Egels. 2002. Digital photogrammetry. Taylor & Francis Inc., New York.

Lane, S.N., R.M. Westaway, and D.M. Hicks. 2003. Estimation of erosion and deposition volumes in a large, gravel-bed, braided river using synoptic remote sensing. Earth Surf. Process. Landforms 28(3):249-271.

Lowe, D.G. 2004. Distinctive image features from scale-invariant keypoints. Int. J. Comput. Vis. 60(2):91-110.

Luhmann, T., S. Robson, S. Kyle, and I. Harley. 2006. Close range photogrammetry: Principles, methods and applications. Whittles Publishing, Hoboken, NJ.

Marzolff, I., and J. Poesen. 2009. The potential of 3D gully monitoring with GIS using high-resolution aerial photography and a digital photogrammetry system. Geomorphology 111(1-2):48-60.

Mikhail, E.M., J.S. Bethel, and J.C. McGlone. 2001. Introduction to modern photogrammetry. John Wiley & Sons, New York.

Momm, H.G., R.L. Bingner, R.R. Wells, J.R. Rigby, and S.M. Dabney. 2013. Effect of topographic characteristics on compound topographic index for identification of gully channel initiation locations. Trans. ASABE 56(2):523-537.

Nachtergaele, J., and J. Poesen. 1999. Assessment of soil losses by ephemeral gully erosion using high-altitude (stereo) aerial photographs. Earth Surf. Process. Landforms 24(8):693-706.

Nouwakpo, S.K., and C. Huang. 2012. A simplified close-range photogrammetric technique for soil erosion assessment. Soil Sci. Soc. Am. J. 76(1):70-84.

Paparoditis, N., and O. Dissard. 2002. 3D data acquisition from visible images. In: M. Kasser and Y. Egels, editors, Digital photogrammetry. Taylor & Francis Inc., New York. p. 168-220.

R Core Team. 2013. R: A language and environment for statistical computing. R Foundation for Statistical Computing, Vienna, Austria.

Rieke-Zapp, D.H., and M.A. Nearing. 2005. Digital close range photogrammetry for measurement of soil erosion. Photogramm. Rec. 20(109):69-87.

Schenk , A.F. 1996. Automatic generation of DEMs. In: C.W. Greve, editor, Digitial photogrammetry: An addendum to the manual of photogrammetry. American Society of Photogrammetry and Remote Sensing, Bethesda, MD. p. 145-150.

Stojic, M., J. Chandler, P. Ashmore, and J. Luce. 1998. The assessment of sediment transport rates by automated digital photogrammetry. Photogramm. Eng. Remote Sens. 64(5):387-395.

Taylor, J.R. 1997. An introduction to error analysis: The study of uncertainties in physical measurements. University Science Books, Sausalito, CA.

Thomas, A.W., R. Welch, and T.R. Jordan. 1986. Quantifying concentrated-flow erosion on cropland with aerial photogrammetry. J. Soil Water Conserv. 41(4):249-252.

Trimble Navigation Ltd. 2013. Trimble R8 GNSS system: Datasheet. trl.trimble.com/dscgi/ds.py/Get/File-140079/022543-079M_TrimbleR8GNSS_DS_0413_LR.pdf (accessed 30 June 2014).

van der Walt, S., S.C. Colbert, and G. Varoquaux. 2011. The NumPy array: A structure for efficient numerical computation. Comput. Sci. Eng. 13(2):22-30.

Warner, W.S. 1995. Mapping a three-dimensional soil surface with hand-held 35 mm photography. Soil Tillage Res. 34(3):187-197.

Welch, R., T.R. Jordan, and A.W. Thomas. 1984. A photogrammetric technique for measuring soil erosion. J. Soil Water Conserv. 39(3):191-194.

Wells, R.R., H.G. Momm, K.R. Gesch, S.M. Dabney, and R.M. Cruse. Quantification of ephemeral gully erosion in Iowa farm fields. In prep.

Wheaton, J.M., J. Brasington, S.E. Darby, and D.A. Sear. 2010. Accounting for uncertainty in DEMs from repeat topographic surveys: improved sediment budgets. Earth Surf. Process. Landforms 35(2):136-156.

Table 1. Uncertainty measures (two standard deviations, 2σ; root mean square error, RMSE; mean absolute error, MAE) of three point cloud elevation quality indicators (spatially averaged elevation change uncertainty, $\delta\Delta Z$; relative vertical accuracy, δZ_{rel}; absolute vertical accuracy, $\delta Z_{\text{geo-ref}}$).

Uncertainty type	Uncertainty metric		
	2σ	RMSE	MAE
$\delta\Delta Z$ (mm)	1.29	0.646	0.537
δZ_{rel} (mm)	0.916	0.457	0.380
$\delta Z_{\text{geo-ref}}$ (cm)	8.26	4.12	3.28

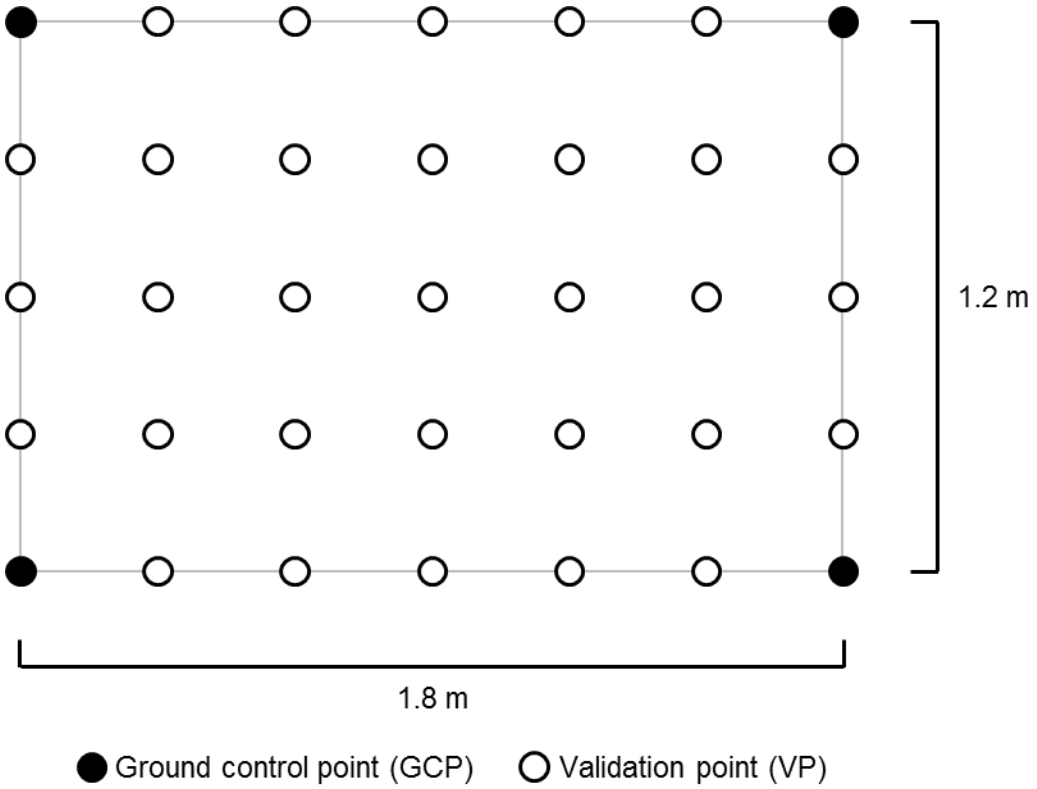

Figure 1. Schematic of experimental reach with four ground control points (GCPs) in corners and 31 validation points (VPs). Target points were placed in a 0.3 m grid. The surveyed GCPs enclosed an area of 2.11 m^2.

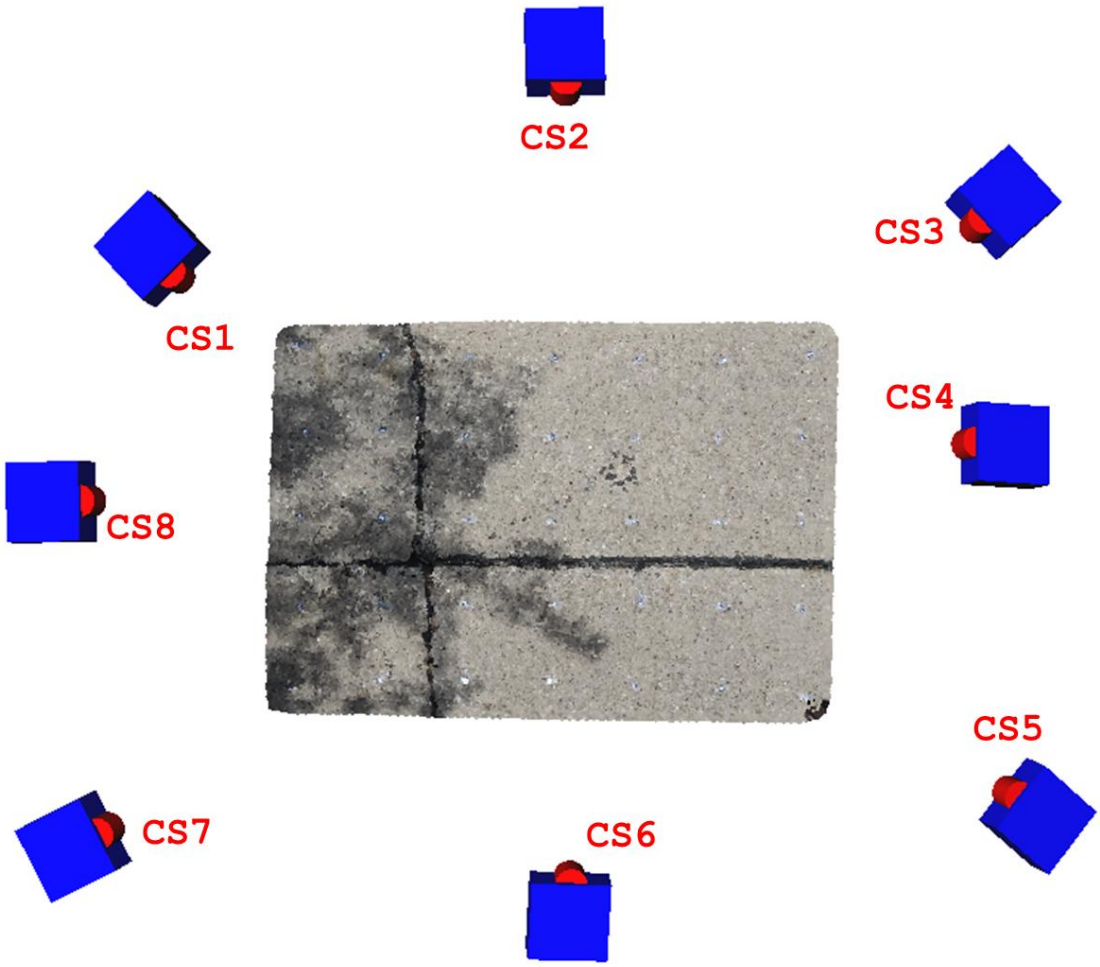

Figure 2. Overhead perspective of camera station (CS) configuration for first sequence (eight photographs) of image acquisition of the experimental surface. CS2 is facing "upstream" and CS6 is facing "downstream."

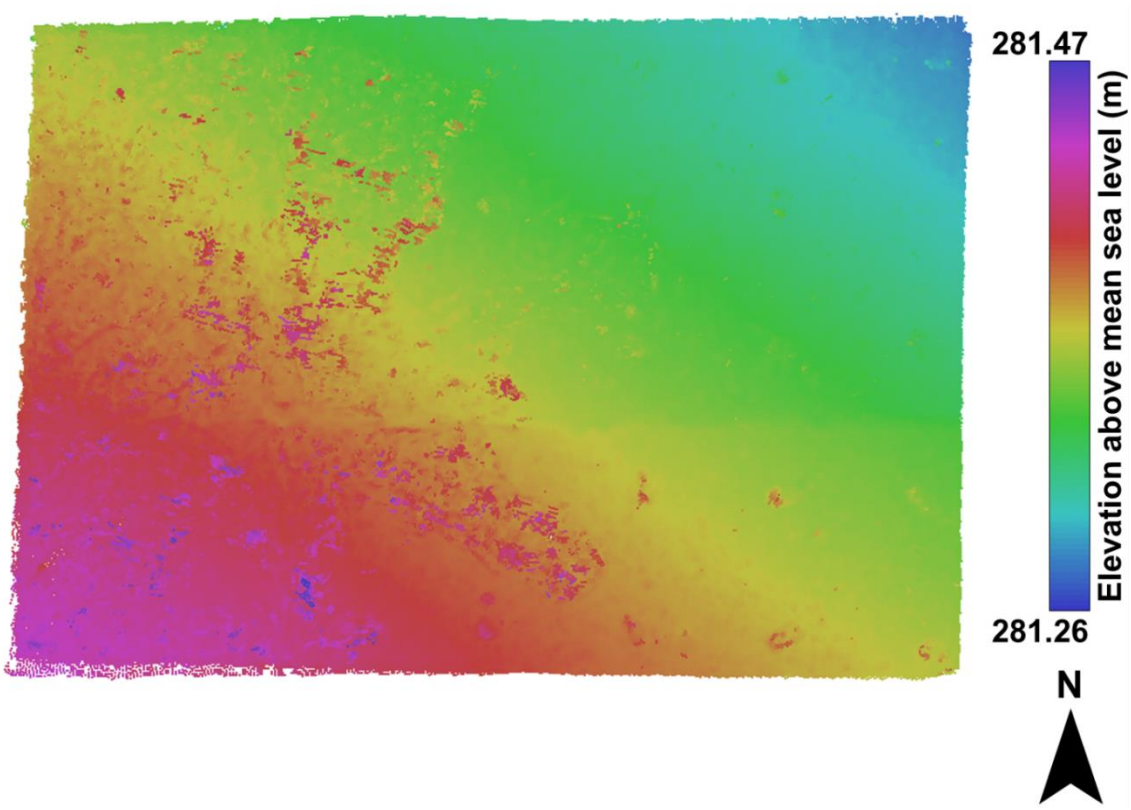

Figure 3. Point cloud of the experimental reach generated with PhotoModeler Scanner from eight images of the asphalt surface. The top of the figure corresponds to the simulated downstream side of the reach.

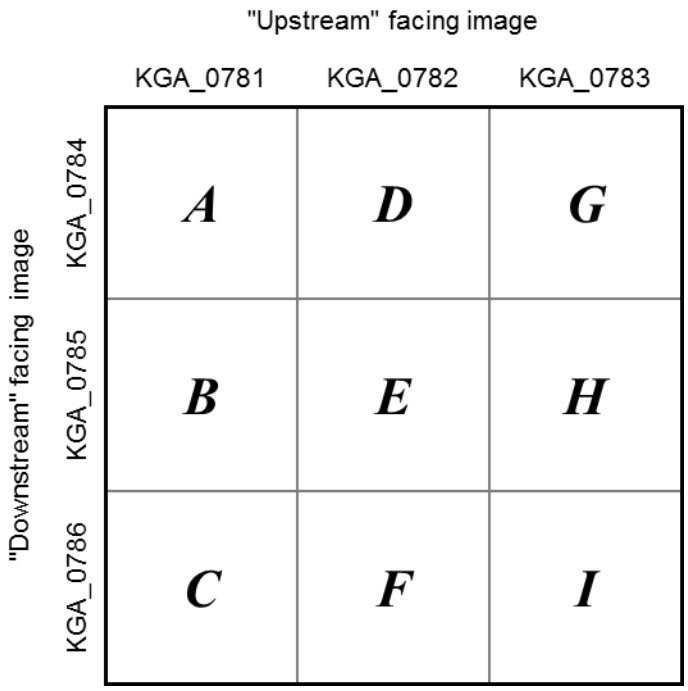

Figure 4. Three "upstream" facing photographs were paired with three "downstream" facing photographs for a total of nine image pairs, *A* through *I*. Each pair was used as input in PhotoModeler Scanner to generate a point cloud (see text for procedure).

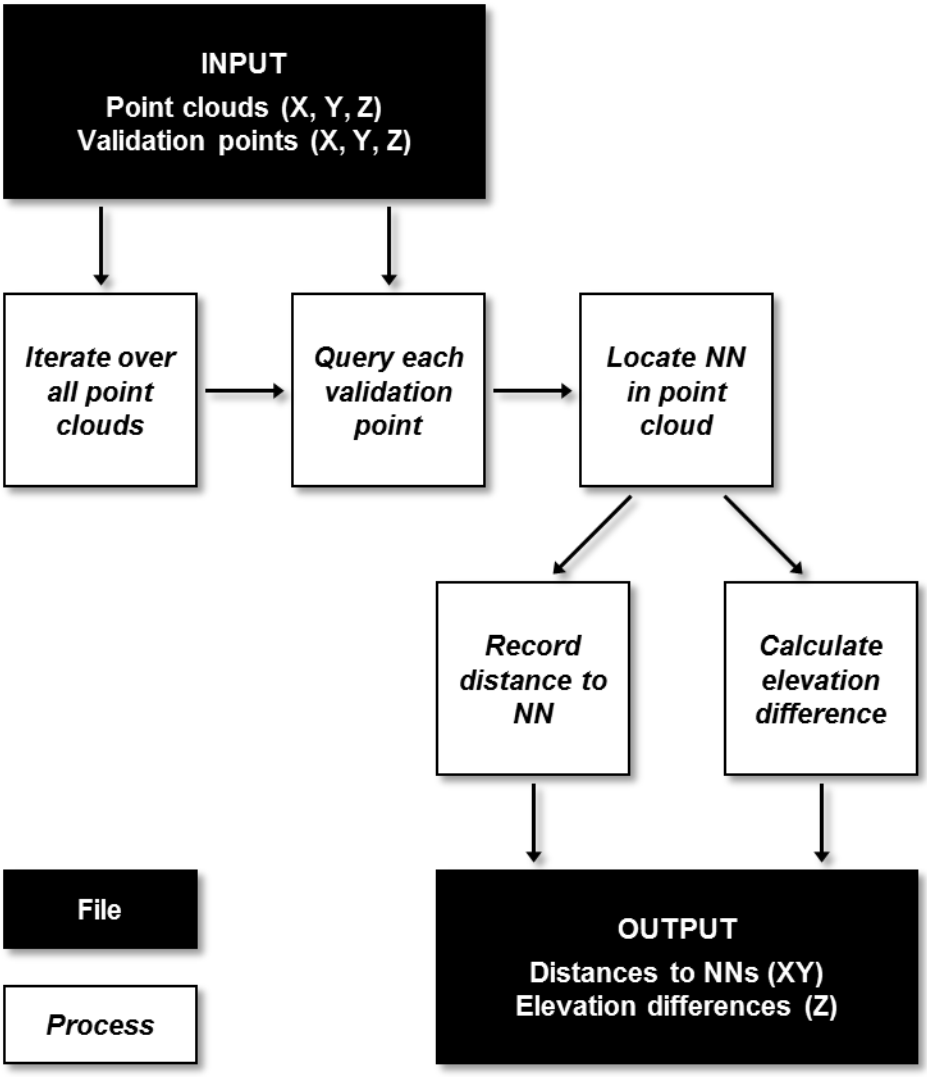

Figure 5. Schematic of the nearest neighbor (NN) search-and-compare algorithm.

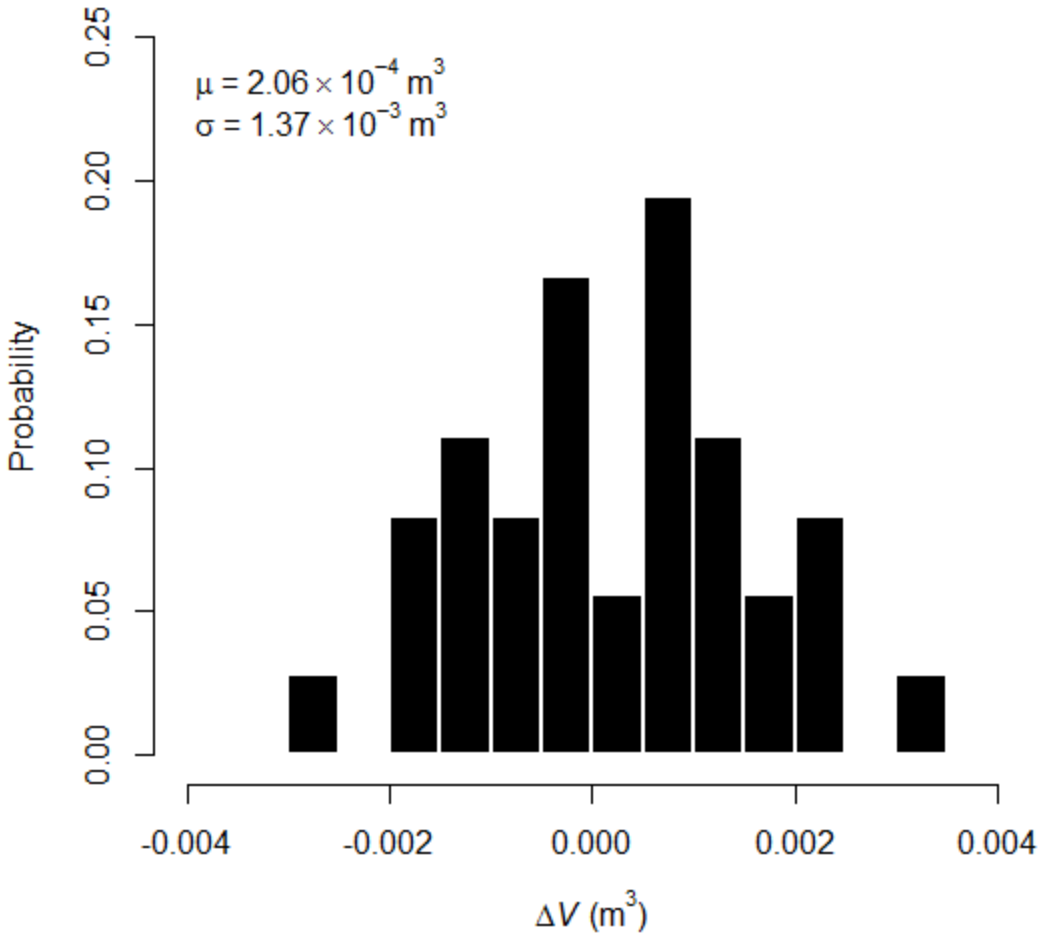

Figure 6. Histogram of volume change ΔV for all comparisons of the photogrammetrically reconstructed experimental asphalt surface using point clouds *A* through *I* as input (n = 36).

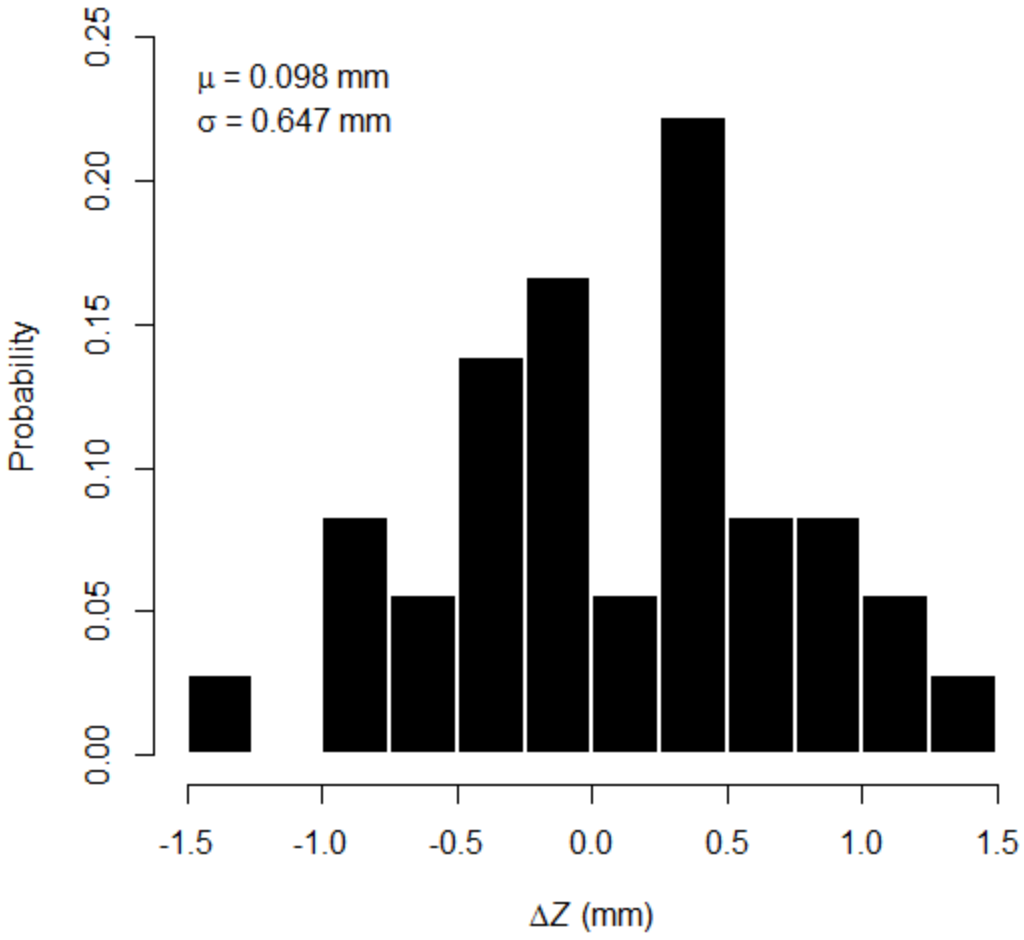

Figure 7. Histogram of average elevation error ΔZ (volumetric discrepancy per reach area) for all comparisons of point clouds *A* through *I* (n = 36).

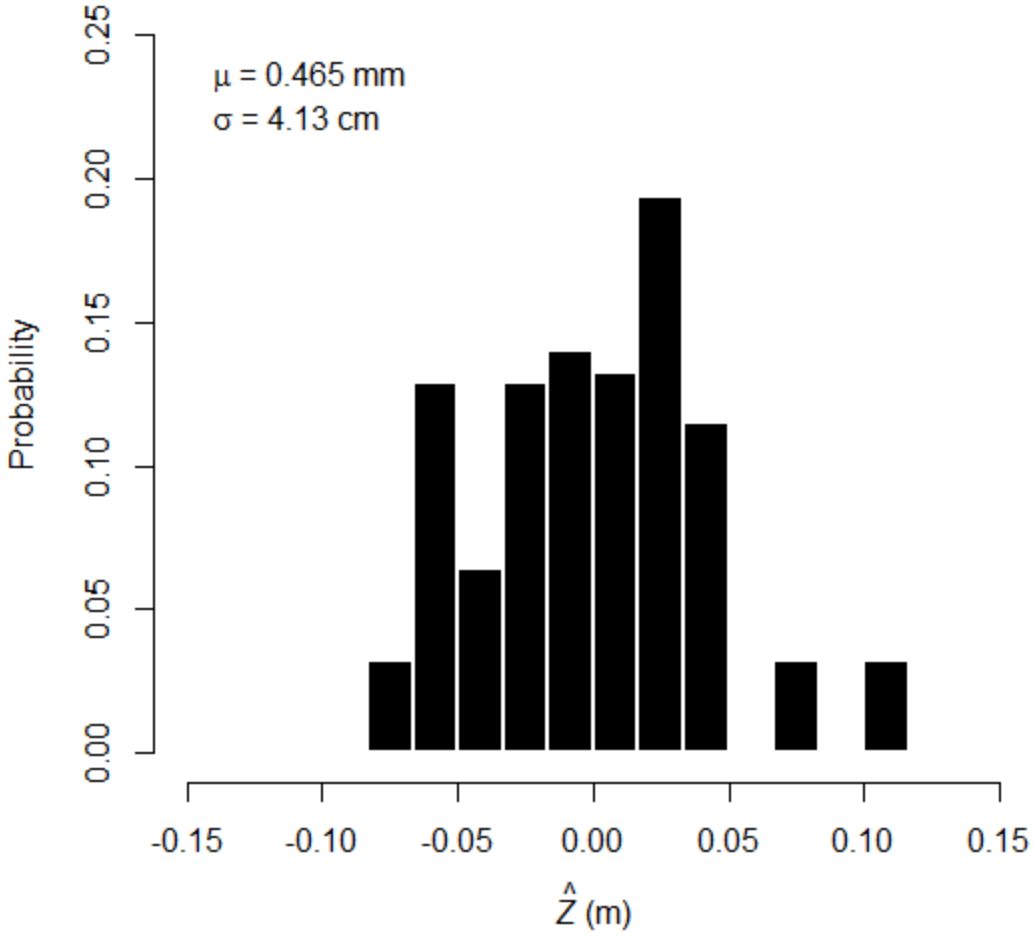

Figure 8. Histogram of elevation discrepancy $\hat{Z}$ (as calculated with Equation 3 by the Python nearest neighbor algorithm) based on all comparisons of 31 validation points with their nearest neighbor in each of the nine point clouds *A* through *I* (*n* = 279).

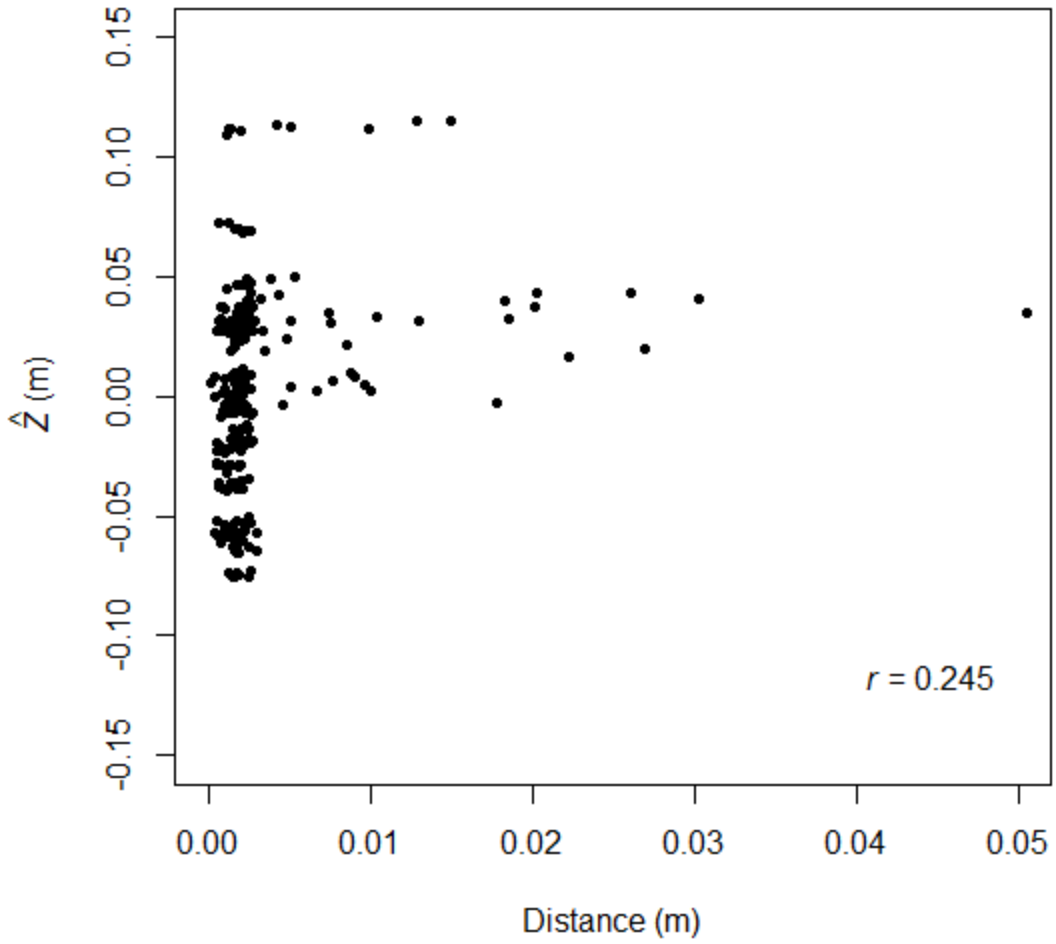

Figure 9. Scatter plot of elevation difference $\hat{Z}$ versus distance from validation point to nearest neighbor (n = 279).

CHAPTER 3

A MULTI-TEMPORAL GEO-REFERENCED TOPOGRAPHIC DATASET OF UPLAND EPHEMERAL CHANNEL DEVELOPMENT

Abstract

Environmental and economic damage by soil erosion is typically worse beyond farm fields than within. Ephemeral gullies are conduits that export eroded soil from agricultural uplands to off-site locations. Because ephemeral gullies develop in non-random landscape locations, they require separate simulation by soil erosion models for conservation planning. This study utilized a recently developed field monitoring approach based on geo-referenced close-range digital photogrammetry to generate a database of morphological reconstructions of ephemeral gullies over multiple time intervals. Combined with a collection of measured soil properties, this topographic ephemeral gully dataset can be used for validation of predictive soil erosion models that explicitly account for erosion by topographically concentrated runoff. The ephemeral channel data were post-processed and used to estimate watershed-scale rates of ephemeral gully erosion of 3.93, 0.847, and 0.415 Mg ha^{-1} for three time intervals. These rates are comparable to expected ranges of soil loss by ephemeral gully erosion in similar landscapes. Although growing plants posed challenges to the method utilized, the reliable data obtained in this study should aid model development and improve soil conservation.

Introduction

Ephemeral gully erosion occurs in agricultural catchments due to topographic convergence of overland flow. Such soil loss negatively impacts agriculture due to decreased crop yields (Martínez-Casasnovas et al., 2005; Cheng et al., 2006) and machinery interference (Casalí et al., 1999). However, the primary consequences of

concentrated flow erosion are typically manifested beyond farm fields because these temporary channels increase landscape drainage network connectivity and allow for efficient transport of soil and agrichemicals from agricultural uplands to downstream reaches and water bodies (Casalí et al., 1999; Gordon et al. 2008). Off-site economic damages due to soil erosion are often greater than on-farm financial losses (Faeth, 1993; Uri, 2000). Because ephemeral gully erosion has a disproportionately large off-farm impact relative to sheet and rill erosion (Poesen et al., 2003), soil conservation measures that specifically combat this phenomenon are critical. While soil conservation planning requires local expertise and cultural practices, soil erosion models also provide a useful tool for conservationists.

Ephemeral gullies have been studied and modeled as distinct landscape features for nearly three decades (e.g. Spomer and Hjelmfelt, 1986; Thomas et al., 1986). These temporary channels have been distinguished from rills on the basis of size, such that a 929 cm^2 cross-sectional area served as the minimum size of an ephemeral gully (e.g. Vandaele et al., 1996; Capra and Scicolone, 2002; Valcárel et al., 2003; Di Stefano and Ferro, 2011). However, this quantitative classification has been gradually replaced with a qualitative distinction: ephemeral gullies remove soil from non-random landscape locations where opposing slopes converge at concave contours whereas rills erode randomly on convex and planar hillslopes (e.g. Bennett et al., 2000; Casalí et al., 2006; De Santisteban et al., 2006; Gordon et al., 2008; Momm et al., 2013; Daggupati et al., 2014). This conceptual definition is favorable because it is well aligned with physically based modeling of ephemeral gully erosion processes.

Sheet and rill erosion are often simulated for soil conservation or research purposes with the Revised Universal Soil Loss Equation 2 (RUSLE2) model (USDA-ARS, 2013) or the Water Erosion Prediction Project (WEPP) hillslope model (Flanagan et al., 1995). RUSLE2 is an empirical model and WEPP is a process model, but neither can be used to simulate ephemeral gully erosion (Bennett et al., 2000; Gordon et al., 2007). RUSLE2 is based on data gathered from runoff plots 22.1 m in length (USDA, 2013), so the lack of a sufficiently large drainage area for channel formation precludes the inclusion of gullies as a source of sediment measured in plot effluent (Vandaele et al., 1996; Boardman 2006). The hillslope component of WEPP is two-dimensional and thus does not account for runoff concentration and the ensuing ephemeral gully erosion; however, the watershed version of WEPP can be configured to model channel erosion process (Flanagan et al., 1995; Ascough et al., 1997), but is used less frequently for soil erosion modelling applications (e.g. Laflen et al., 2004). The Ephemeral Gully Erosion Model (EGEM) was developed specifically to simulate this distinct process (Woodward, 1999), but EGEM has been shown to perform poorly and has severe limitations (Nachtergaele et al., 2001; Capra et al., 2005).

Recent improvements in watershed-scale modelling of ephemeral gullies have been made (Momm et al., 2012; Momm et al., 2013; Daggupati et al., 2014). However, field-scale simulations have not advanced at the same pace. Gordon et al. (2007; 2008) successfully used Annualized Agricultural Non-Point Source (AnnAGNPS) to model ephemeral gully erosion. Coupling RUSLE2 with a physically based tool such as the Chemicals, Runoff, and Erosion from Agricultural Management Systems (CREAMS) model constitutes another viable approach to estimate total soil erosion within a field

(Dabney et al., 2011; Dabney et al., 2012). Dabney et al. (2014) have developed the Ephemeral Gully Erosion Estimator (EphGEE) model; implemented it in the context of total field-scale erosion including sheet, rill, channel, and tillage erosion; and achieved reliable long-term results. These recently applied models and any future developments would benefit from a topographic dataset of ephemeral gully erosion that can be used for validation and calibration.

Field measurements are a requirement for accurate simulation of channel erosion (Stroosnijder, 2005). Field-scale observations of soil erosion also occupy an under-studied void between watershed-scale and plot-scale measurements that are made far more frequently (Poesen et al., 1996; Deasy et al., 2011). The preferred method to measure field-scale soil erosion is quantification of change in gully morphology (Lal, 2001; Stroosnijder, 2005). Morphological data of developing ephemeral channels should be gathered from multiple fields over multiple years, should be geo-referenced and in a digital format for efficient incorporation into pre-existing digital elevation models (DEMs), and must be sufficiently reliable to allow for accurate representation of actual geomorphic change. There is a pressing need for such field measurements of ephemeral gully erosion due to a lack of suitable data to aid model development (Dabney et al., 2011).

The importance of developing appropriate field methods to monitor ephemeral gully development in addition to improving predictive model capability has been emphasized (Poesen et al., 2003). Castillo et al. (2012) compared a suite of techniques that are available to quantify gully morphology. Simple approaches include measuring tape (Zhang et al., 2007; Capra et al., 2009) or a pole (Castillo et al., 2012) to measure

depths and widths of triangle or quadrilateral cross-sections. Profile meters present a technique to sample cross-section depths at denser intervals (Leatherman, 1987; Casalí et al., 1999; Bennett et al., 2000; Casalí et al., 2006; De Santisteban et al., 2006; Di Stefano and Ferro 2011). Real-time kinematic global positioning system (RTK-GPS) survey (Cheng et al., 2006; Wu et al., 2008) and total station survey (Castillo et al., 2012) have been used to obtain gully morphology. Other close-range techniques to reconstruct channels include laser profilers (Giménez et al., 2009; Castillo et al., 2012) and ground based light detection and ranging (LiDAR) scanners (Momm et al., 2011; Castillo et al., 2012; Nouwakpo and Huang, 2012). Finally, close-range photogrammetry can be employed to generate high-resolution gully reconstructions.

Photogrammetry can be applied remotely or proximally. Aerial photogrammetry (object distance > 10 m) has been used to assess gully development (Thomas et al., 1986; Nachtergaele and Poesen, 1999; Giménez et al., 2009; Marzolff and Poesen, 2009), but the high ground area-to-pixel area ratio constrains the horizontal resolution of the resultant photogrammetric DEM. A relatively lower ground area-to-pixel area ratio is achievable with close-range images, which are obtained with ground-based cameras. Closer imagery thus yields greater horizontal DEM resolution due to computation of denser point clouds. Such three-dimensional detail on the order of 10^{-2} to 10^{-3} m is required to accurately assess small geomorphic changes in ephemeral gullies. As such, an increasing number of researchers (Rieke-Zapp and Nearing, 2005; Gessesse et al., 2010; Heng et al., 2010; Castillo et al., 2012; Gordon et al. 2012; Nouwakpo and Huang, 2012; Gómez-Gutiérrez et al., 2014; Kaiser et al., 2014; Wells et al., in prep.) have utilized close-range photogrammetry for soil erosion research over the last decade.

The research presented in this chapter has applied a technique developed by Wells et al. (in prep.) that couples RTK-GPS survey and close-range photogrammetry to generate geo-referenced point clouds of ephemeral gullies in multiple agricultural fields over longer time intervals than are currently documented. Ephemeral gullies were photographed for compilation of a photogrammetric dataset, which was complemented by a dataset of soil properties. The objective of this study was to generate a database of ephemeral gully morphologies and soil parameters suitable for model validation and to derive field-scale estimates of ephemeral gully erosion rates.

Methods

Study Site

Field research was conducted during 2013 and 2014 at Neal Smith National Wildlife Refuge in Jasper County, Iowa, USA (Figure 1). Twelve field-scale ephemeral watersheds were established in 2007 (*cf*. Helmers et al., 2012). The experimental watersheds measure 0.47 to 3.19 ha with 6.1% to 10.5% average slopes, are managed under a no-till 2 y maize–soy rotation (2013: soy; 2014: maize) with varying areal proportions removed from crop production for prairie reconstruction, and are identified as Interim 1 through 3, Orbweaver 1 through 3, and Basswood 1 through 6 (Helmers et al., 2012). Any channels that developed in topographic swales after 2007 were filled in March 2012. Precipitation data were originally obtained from the MesoWest meteorological database maintained by the University of Utah Department of Atmospheric Sciences (UUDAS, 2014), and then verified with precipitation information from the Iowa Daily Erosion Project (IDEP) website (Cruse et al., 2006).

In April 2013, monitoring sites were established along the thalweg of each of the 12 zero-order watersheds where there was visible evidence of erosion due to concentrated overland flow. In each watershed, the sites were placed sequentially along the concentrated flowpaths and were spaced approximately 10 m apart (Figure 2). A total of 88 sites were maintained through 2014 (Table 1). A 1.8 m by 1.2 m PVC frame was used to locate four survey stakes that demarcated the extents of each monitoring site, which occupied an average area of 2.16 m^2 (Figure 3). These stakes were surveyed with RTK-GPS initially and again in May 2014 to avoid measurement errors due to potential freeze-thaw dislocation. The surveyed stakes were used as ground control points (GCPs) to geo-reference and scale photogrammetric point clouds.

Photogrammetry & Post-Processing

An established procedure was followed to photograph each monitoring site (Wells et al., in prep.). A calibrated Nikon D7000 digital single-lens reflex camera with an AF Nikkor lens of 20 mm focal length (fixed) and f/2.8D aperture was used for all photography. All image files were saved in JPEG format. To capture images of each monitoring site, the camera was mounted to an aluminum arm attached to a frame backpack worn by the operator and was viewed with an iPad connected to the camera via a Cam Ranger wireless router (Wells et al., in prep.). Each site was photographed twice: from downstream facing upstream (parallel to the channel) and vice versa (Figure 4).

Image pairs were imported to PhotoModeler Scanner (Eos Systems Inc., 2014) to generate a point cloud for each site. PhotoModeler Scanner uses algorithms based on the scale-invariant feature transform (SIFT) developed by Lowe (2004) to identify matching pixels in the two photographs and automatically solve for the location of both cameras in

three-dimensional image space (Figure 5). The four GCPs are then manually identified and registered with survey data in order to transform image space into object space and geo-reference the entire model. The matching points identified by the SIFT algorithm are then sampled at 5 mm density to compute a point cloud with the Create Dense Surface stereo image pair option. The final geo-referenced point cloud is exported as a *.txt file (Figure 6).

The monitoring sites were visited periodically during the 2013 and 2014 growing seasons in order to generate multiple point clouds for each site (Table 1). The same protocol is followed for field-work and computer processing to create every point cloud (Figure 7). In order to assess erosive (or depositional) changes within each monitoring site, sequential pairs of point clouds were post-processed using custom Python code developed by Wells et al. (in prep.). The algorithm interpolates both point clouds to a 5 mm grid DEM and uses the elevation difference of corresponding raster cells from the two time steps (Figure 8) to compute the total volume change within the monitoring site between the photography dates (Wells et al., in prep.). Cross-section and longitudinal profiles are also outputted graphically (Figure 9) and as *.csv tables (Wells et al., in prep.).

Soil Properties

In addition to tabular cross-section profile data, soil properties were also measured to facilitate future model development and refinement. Particle size distribution, total organic carbon, and bulk density have been measured to assess the relationships between soil and ephemeral gully erosion (Lentz et al., 1993). The soil properties measured herein included bulk density, texture, soil carbon, and wet aggregate

stability. For each watershed block (Basswood, Interim, Orbweaver), soil properties were measured in one watershed (Basswood 1, Interim 3, Orbweaver 1) at five locations: within the channel in the bottom half of the channel (C_b), in the channel within the top half of the channel (C_t), gully bank at bottom (B_b), gully bank at top (B_t), and a control (Con) located at least 10 m away from the concentrated flowpaths at an intermediate elevation.

Bulk density was sampled at a higher spatial frequency in order to determine an overall average value for each block. Soil cores were taken to 7.6 cm depth with a double-cylinder sampler (Grossman and Reinsch, 2002) in all 12 watersheds sequentially along channels within a few paces from monitoring sites. Samples were obtained on August 8, 2013 (n = 31), and again on June 10, 2014 (n = 46). Cores were oven dried at 105°C for 24 h and then weighed to determine bulk density, which was averaged for each block. These bulk density samples corresponded to gully bank locations (B_b and B_t) and were used as such. Additional bulk density measurements (n = 24) were made on June 24, 2014 at the C_b, C_t, and Con sites in each block.

Soil samples were obtained at 15 locations (C_b, C_t, B_b, B_t, and Con in each block) on June 24, 2014 for measurement of the remaining soil properties. At each location, a 3.2 cm diameter probe was inserted to 15 cm depth five times to make a composite sample. Particle size analysis was conducted according the pipette method (Gee and Or, 2002). Total soil carbon and soil organic matter were determined by combustion. A modified approach of Nimmo and Perkins (2002) was followed to quantify wet aggregate stability. First, field-moist samples were passed through an 8 mm sieve and air-dried. Samples were then wetted slowly with filter paper to a gravimetric water content of 40 g

H_2O g^{-1} dry soil. Moist samples were then placed onto a set of sieves (4, 2, 1, 0.5, and 0.25 mm). Each sieve stack was submerged in water and vertically shaken at 128 revolutions min^{-1} for 5 min. The aggregates remaining on each sieve were oven dried at 65°C over night and then weighed.

Ephemeral Gully Erosion

The primary motivation for applying photogrammetry to reconstruct multi-temporal ephemeral gully morphologies is to improve predictive capabilities of soil erosion models. However, it is worthwhile to use the calculated volume changes in monitoring sites to estimate total volumetric change of entire channels between two time steps. Doing so allows for verification that site-scale observations (approximately 2 m^2) are plausible when translated to the field-scale (three to four orders of magnitude larger). To determine total ephemeral gully volumetric change, volume changes within observed sites (computed) were used to estimate volume changes between sites (interpolated).

Interpolation was necessary because monitored reaches were spatially discontinuous (Figure 2). The interpolation procedure was based on a modification of the end area method (EAM), which is a well-documented approach to estimate gully volume using sequential cross-sectional area measurements (Spomer and Hjelmfelt, 1986; Capra and Scicolone, 2002; Casalí et al., 2006; De Santisteban et al., 2006; Zhang et al., 2007; Capra et al., 2009; Di Stefano and Ferro, 2011; Capra et al., 2012; Castillo et al., 2012). The EAM calculates total gully volume V as

$$V = \sum_{i=1}^{n} V_i = \sum_{i=1}^{n} 0.5(C_{i-1} + C_i) \times L_i \quad (1)$$

where i is the segment between two cross-sections, n is the number of segments, V_i is the volume of segment i, C_{i-1} is the downstream cross-sectional area, C_i is the upstream

cross-sectional area, and L_i is the length of the segment measured between the cross-sections. Equation 1 assumes a linear change in morphology between cross-sections, and this assumption of linearity was also followed for the modified EAM.

Post-processing of sequential point clouds yields volume change over the time interval (Wells et al., in prep.), but only for photographed channel reaches. To determine volume change between monitored sites, the average elevation changes within the upstream and downstream sites are averaged and then multiplied by the corresponding ground area between photographed reaches. The sums of volumetric changes inside the observed sites and within the interpolated spaces are added to yield the total volume change of a channel ΔV_c given as

$$\Delta V_c = \sum_{i=1}^{n} \Delta V_i + \sum_{i=1}^{n-1} 0.5 \left(\frac{\Delta V_i}{A_i} + \frac{\Delta V_{i+1}}{A_{i+1}} \right) \times A_b \qquad (2)$$

where i is a monitored site, n is the number of sites experiencing channel erosion, ΔV_i is the volume change within site i, A_i is the area of site i, ΔV_{i+1} is the volume change within the site immediately upstream of site i, A_{i+1} is the area of the upstream site, and A_b is the ground area between site i and its upstream neighbor. The interpolation procedure is illustrated in Figure 10. All areas were measured with ArcMap 10 (ESRI, 2010).

To assess the plausibility of estimated total volume changes within the observed channels, ΔV was converted to mass flux, ΔM, using topsoil (7.6 cm) bulk density, ρ_b (e.g. Woodward, 1999; Zhang et al., 2007). Bulk density was assumed to be uniform in space and time for this calculation. Mass flux was divided by both channel area and field area (i.e. channel drainage area) to determine the rate of ephemeral gully erosion over each time interval. Erosion rate (mass flux) uncertainty was defined by combining the individual uncertainties in volume calculations and bulk density measurements. The

errors in ΔV and ρ_b are assumed to be independent and random, so Taylor (1997) Equation 3.18 allows the uncertainty of mass flux $\delta\Delta M$ to be determined for each ephemeral gully by

$$\delta\Delta M = |\Delta M| \times \sqrt{\left(\frac{\delta\Delta V}{\Delta V}\right)^2 + \left(\frac{\delta\rho_b}{\rho_b}\right)^2} \quad (3)$$

where ΔM is the estimated mass flux within a channel, ΔV is the volume change, ρ_b is the bulk density, and $\delta\Delta V$ and $\delta\rho_b$ are the 2σ uncertainties in volume change and bulk density, respectively. $\delta\Delta V$ for each channel was computed by multiplying the $\delta\Delta Z$ value of ± 1.29 mm (Chapter 2) by the channel ground area.

Results

Concentrated flow erosion occurred in nine of the 12 experimental watersheds during 2013 and 2014, ephemeral gully lengths ranged 18.9 to 137.2 m, and channel density was between 15.3 and 87.3 m ha^{-1} (Table 2). Average bulk density values for each block were lower in 2014 than in 2013 by an overall difference 0.17 Mg m^{-3} ($p <$ 0.01; Table 3). Other soil properties are summarized in Table 4. No soil properties significantly differed (based on comparison of 95% confidence intervals) by sampling position (i.e. channel, bank, bottom, top, and control). Bulk density was numerically higher in channel thalwegs relative to that on gully banks, higher in lower watershed reaches than in upper reaches, and highest at the control location. Lower field reaches had relatively higher sand content. Total soil carbon and soil organic matter were numerically greater on channel banks than within the gullies and were highest for the control samples. Soil aggregates were slightly more stable at upper reaches than at lower locations within

the fields, and aggregate stability was substantially higher at the control sampling sites than at all other locations.

Volume changes within monitored sites were used to derive rates of ephemeral gully erosion. Channel volume change, estimated mass flux, mass flux per channel area, and mass flux per watershed area are listed in Tables 5, 6, 7, and 8 for each field that experienced concentrated flow erosion during the four time intervals (T_0 to Tt_1: April 25, 2013 to June 10, 2013; T_1 to T_2: June 10, 2013 to September 24, 2013; T_3 to T_4: May 14, 2014 to May 29, 2014; and T_4 to T_5: May 29, 2014 to June 5, 2014) for which corresponding multi-temporal surface reconstructions were available. According to MesoWest, rainfall during the first, second, and fourth time intervals was 232.4, 159.5, and 37.8 mm, respectively; precipitation details were unavailable for the third interval due to a reset of the rain gauge. IDEP data indicated similar values, with approximate rainfall depths of 250, 150, 10, and 30 mm for the four time intervals. The average computed rates of ephemeral gully erosion on the per channel area basis for each time interval (T_0 to T_1, T_1 to T_2, T_3 to T_4, and T_4 to T_5) were 306.1, 76.3, 50.5, and –51.6 Mg ha^{-1}, respectively; the average calculated rates of soil loss by topographically concentrated runoff on the per gully drainage area basis for the four time intervals were 3.93, 0.847, 0.415, and –0.493 Mg ha^{-1}. Calculations for average rates only include significant changes (i.e. computed net mass flux must be larger than the uncertainty).

Discussion

Photographs obtained of the ephemeral gully monitoring sites at Neal Smith National Wildlife Refuge constitute a permanent digital record of the soil surfaces observed during this study. Images were the primary raw data collected, but the point

clouds generated therewith comprise a secondary collection of data that describe the studied channels. Volume changes and channel profiles extracted from post-processing are the most derived and readily useful data.

Erosion estimates were made for the four time intervals T_0 to T_1, T_1 to T_2, T_3 to T_4, and T_4 to T_5 based on volume changes computed during point cloud post-processing. For each post-processing run, spreadsheets of cross-section and longitudinal profiles of the monitoring sites for both the initial and end dates were generated. These spreadsheets can be integrated into predictive models for calibration. Because the topographic data in these spreadsheets are geo-referenced, they may be easily incorporated into pre-existing terrain models. The multi-temporality of the channel morphology data allows for inverse modeling of ephemeral gully evolution. Despite this, the temporal resolution is insufficient to use for simulation of the processes of concentrated flow erosion such as headcut erosion (Wells et al., 2009; Wells et al., 2010) or channel widening (Wells et al., 2013).

Ephemeral gullies formed in nine of 12 fields monitored in this study. The three fields in which channels did not develop (Basswood 2, Basswood 3, Orbweaver 2) had gentler slopes (6.7%), smaller drainage areas (2.40 ha), or shorter maximum slope lengths (220 m), where the maximum value of the three fields without channels is given in parentheses (Table 2). This is consistent with the concept that there exist slope and area thresholds for the initiation of ephemeral gullies (Vandaele et al., 1996; Capra and Scicolone, 2002; Poesen et al., 2003; Valentin et al., 2005; Daggupati et al., 2014). Channel length was moderately well correlated with watershed drainage area (r = 0.855) and watershed maximum slope length (r = 0.879). Of the other landscape parameters and

soil properties, average slope was most often the explanatory variable best-correlated with volume change and mass flux from the channels. These general relationships, while statistically inconclusive, imply that larger drainage area, greater slope length, and steeper slope increase likelihood of ephemeral gully development, channel length, and sediment export. However, the correlations in this study are moderate at best, which suggests that different or more complex topographic (e.g. compound topographic index) or soil (e.g. critical shear stress, concentrated erodibility) parameters could be better predictors of the degree or magnitude of ephemeral gully erosion.

The soil properties compiled in Table 4 can be used to specify primary parameters (or to derive secondary parameters with pedotransfer functions) within gully erosion models. The soil dataset collected for this research had no correlation with ephemeral gully volume or sediment movement. Channel lengths were modestly correlated with soil texture: sand (r = 0.785), silt (r = –0.808), and clay (r = 0.733). Further detection of significant relationships between soil and ephemeral gully morphology may be due to small sample size (n = 15) or the lack of actual associations between soil and channel characteristics.

For the soil properties determined by location, it is logical that channel thalwegs had greater bulk density and lesser total carbon and organic matter relative to other sampling locations. The samples obtained from within the ephemeral gullies contained more subsoil (instead of more topsoil, such as the samples taken on gully banks or at the control locations), and thus the larger bulk density and lower carbon content. Bulk density was largest at the control location, which is plausible because the soil near and within the channels is less consolidated due to repeated displacement by topographically

concentrated runoff. Likewise, and perhaps most important, aggregate stability was highest at the control location. Soil aggregates on channel banks and within ephemeral gullies may be less stable due to the force exerted by flowing water. Conversely, the lower bulk density and less stable aggregates near and in channels may promote erosion because the soil is weaker and less consolidated. A reinforcing feedback between the two scenarios is likely.

In addition to terrain and soil characteristics, ephemeral gully erosion is also influenced by management. The fields were not tilled during the study period. Relative to tillage, no-till management reduces sheet and rill erosion relatively more than runoff (Dabney et al., 2012). Despite minimal anthropogenic soil disturbance, sufficient occurrence of topographic runoff concentration and the ensuing channel scouring allowed ephemeral gullies to form.

The average ephemeral gully erosion rates for all four time steps are higher when reported per channel area than when divided by the total areas of the zero-order watersheds. The per-field-area figures are in addition to sheet and rill erosion that could be computed with RUSLE2 or WEPP, whereas the per-channel area values are highly localized and therefore difficult to evaluate. It should be noted that the channel area utilized includes the overbank area captured in the photographs of each monitoring site. Because the monitored channels did not fill the sites (ground areas within sets of four survey stakes), the channel areas are overestimates. Further, the volume changes computed during post-processing did not discriminate between channels and floodplains, so morphological development outside of the gullies within each site impacted the calculation of volume change. Channels could be automatically separated from overbank

areas with an edge detection algorithm (Wells et al., 2013). However, the computed volumetric change within monitored channel reaches allowed for estimation of total channel volumes with Equation 2, which in turn permitted a means for quantitative data verification.

The average field-scale rates of ephemeral gully erosion for time intervals T_0 to T_1, T_1 to T_2, and T_3 to T_4 were 3.93, 0.847, and 0.415 Mg ha^{-1}, respectively. The value for the T_0 to T_1 interval is larger because it only reflects the ephemeral gully erosion rates of two fields, one (Interim 3) of which experienced the most erosion. The value was lesser for the T_1 to T_2 interval due to less rainfall (150 mm) than the previous interval (250 mm), and the small value for the T_3 to T_4 interval is attributed to the much shorter elapsed time (15 d) with little precipitation (about 10 mm). The magnitudes of ephemeral gully erosion for the first three time intervals compare well with (i) the average Iowa annual ephemeral gully erosion rate under no-till of 4.00 ± 1.76 Mg ha^{-1} simulated by Gordon et al. (2008), (ii) the range in Iowa annual ephemeral gully erosion of 2 to 18.2 Mg ha^{-1} compiled by Poesen et al. (2003), and (iii) the average annual sediment yield of 8.30 ± 3.21 Mg ha^{-1} from 2007 to 2010 from the 100% row-crop watersheds at Neal Smith National Wildlife Refuge reported by Helmers et al. (2012). The contribution of upland channel erosion to total soil losses in Iowa ranges from 19% to 45% (Poesen et al., 2003). This range combined with the lower (5.09 Mg ha^{-1}) and upper (11.51 Mg ha^{-1}) bounds of sediment delivery from 100% row-crop fields (Helmers et al., 2012) yields a range of 0.967 to 5.180 Mg ha^{-1} of ephemeral gully erosion within the experimental watersheds at Neal Smith National Wildlife Refuge. The rates of upland ephemeral channel erosion of 3.93, 0.847, and 0.415 Mg ha^{-1} for the first three time intervals are therefore deemed

plausible because the morphological changes at the observation scale are realistic when extrapolated to the field (gully drainage area) scale. Furthermore, the expected rates of 0.967 to 5.180 Mg ha^{-1} are based on runoff data collected from late March through late November (Helmers et al., 2012), so less soil loss would have occurred (per unit time) had those longer time intervals been separated into finer temporal increments.

The derived estimate of average field-scale ephemeral gully erosion for the final time interval T_4 to T_5 of –0.493 Mg ha^{-1} requires separate interpretation. The negative value implies average net deposition within all channels due to positive volumetric changes within the photographed monitoring sites. Rather than substantial accumulation of displaced soil, the supposed deposition reflects the vertical growth of the maize crop within each monitoring site. This interference of crops is one major challenge to the method used in this field study.

In 2014, Orbweaver 1 contained extensive weed growth. The monitoring sites in Orbweaver 1 were photographed and point clouds were generated, but substantial vertical noise and horizontal gaps in the point clouds precluded accurate post-processing for volume change calculation and profile extraction. In a similar manner, in 2013 the September 24 photography was only made possible by removing the soy crop within the monitoring sites prior to image acquisition. In 2014, photography was suspended after June 5 due to rapid growth of the maize crop and occlusion of the imaging surface by the vegetative canopy. The close-range photogrammetric technique is therefore best applied to fallow landscapes or to monitoring sites that do not contain actively growing biomass.

Despite the challenges presented by crop and weed interference, the utilized method has numerous benefits. The data quality is good because vertical uncertainty is

low (Chapter 2) and horizontal resolution is high (5 mm), and the data are of high utility because they are geo-referenced and easily integrated into computer applications. The in-field data collection approach is advantageous because it is repeatable (necessary for multi-temporal surface reconstruction) and fast (one researcher was able to travel to Neal Smith National Wildlife Refuge [1 h, one way] and photograph all monitoring sites in less than 6 to 8 h). Point cloud generation and post-processing adhere to a workflow that minimizes subjectivity (Wells et al., in prep.). As long as plant interference is minimal and both images of a given monitoring site clearly contain all four GCPs, geo-referenced close-range digital photogrammetry provides an efficient and effective method to reconstruct a time series of ephemeral channel morphologies.

Conclusions

A multi-temporal morphological dataset of ephemeral gullies was successfully produced with repeated application of geo-referenced close-range photogrammetry to monitoring sites in 12 fields at Neal Smith National Wildlife Refuge in Iowa, USA. Observed reaches of ephemeral channels were photographed six times during 2013 and 2014, which allowed for the generation of digital surface reconstructions in the form of point clouds for each imaging date. Point cloud post-processing outputted tables of cross-section and longitudinal profiles of ephemeral gullies that can be used for model validation, and multi-temporal channel topographic data were supplemented by a dataset of soil properties that may further enhance model parameterization. The estimated rates of ephemeral gully erosion per drainage area for three time intervals were 3.93, 0.847, and 0.415 Mg ha^{-1}, which are plausible with respect to previously measured and modeled rates in Iowa. This consistency of extrapolated field-scale estimates of ephemeral gully

erosion implies that the micromorphological changes calculated from the observation scale are appropriate representations of actual geomorphic changes due to ephemeral channel development.

References

Ascough, J.C., C. Baffaut, M.A. Nearing, and B.Y. Liu. 1997. The WEPP watershed model: I. Hydrology and erosion. Trans. ASAE 40(4):921-933.

Bennett, S.J., J. Casalí, K.M. Robinson, and K.C. Kadavy. 2000. Characteristics of actively eroding ephemeral gullies in an experimental channel. Trans. ASABE 43(3):641-649.

Boardman, J. 2006. Soil erosion science: Reflections on the limitations of current approaches. Catena 68(2-3):73-86.

Capra, A., and B. Scicolone. 2002. Ephemeral gully erosion in a wheat-cultivated area in Sicily (Italy). Biosyst. Eng. 83(1):119-126.

Capra, A., L.M. Mazzara, and B. Scicolone. 2005. Application of the EGEM model to predict ephemeral gully erosion in Sicily, Italy. Catena 59(2):133-146.

Capra, A., P. Porto, and B. Scicolone. 2009. Relationships between rainfall characteristics and ephemeral gully erosion in a cultivated catchment in Sicily (Italy). Soil Tillage Res. 105(1):77-87.

Capra, A., V. Ferro, P. Porto, and B. Scicolone. 2012. Quantifying interrill and ephemeral gully erosion in a small Sicilian basin. Zeitschrift für Geomorphologie 56(1):9-25.

Casalí, J., J.J. López, and J.V. Giráldez. 1999. Ephemeral gully erosion in southern Navarra (Spain). Catena 36(1-2):65-84.

Casalí, J., J. Loizu, M.A. Campo, L.M. De Santisteban, and J. Álvarez-Mozos. 2006. Accuracy of methods for field assessment of rill and ephemeral gully erosion. Catena 67(2):128-138.

Castillo, C., R. Pérez, M.R. James, J.N. Quinton, E.V. Taguas, and J.A. Gómez. 2012. Comparing the accuracy of several field methods for measuring gully erosion. Soil Sci. Soc. Am. J. 76(4):1319-1332.

Cheng, H., Y. Wu, X. Zou, H. Si, Y. Zhao, D. Liu, and X. Yue. 2006. Study of ephemeral gully erosion in a small upland catchment on the Inner-Mongolian Plateau. Soil Tillage Res. 90(1-2):184-193.

Cruse, R., D. Flanagan, J. Frankenberger, B. Gelder, D. Herzmann, D. James, W. Krajewski, M. Kraszewski, J. Laflen, J. Opsomer, and D. Tody. 2006. Iowa Daily Erosion Project. http://wepp.mesonet.agron.iastate.edu (accessed 24 November 2014). In: Daily estimates of rainfall, water runoff, and soil erosion in Iowa. J. Soil Water Conserv. 61(4):191-199.

Dabney, S.M., D.C. Yoder, D.A.N. Vieira, and R.L. Bingner. 2011. Enhancing RUSLE to include runoff-driven phenomena. Hydrol. Process. 25(9):1373-1390.

Dabney, S.M., D.C. Yoder, and D.A.N. Vieira. 2012. The application of the Revised Universal Soil Loss Equation, Version 2, to evaluate the impacts of alternative climate change scenarios on runoff and sediment yield. J. Soil Water Converv. 67(5):343-353.

Dabney, S.M., D.A.N. Vieira, D.C. Yoder, E.J. Langendoen, R.R. Wells, and M.E. Ursic. 2014. Spatially distributed sheet, rill, and ephemeral gully erosion. J. Hydrol. Eng. C4014009:1-12.

Daggupati, P., A.Y. Sheshukov, and K.R. Douglas-Mankin. 2014. Evaluating ephemeral gullies with a process-based topographic index model. Catena 113:177-186.

De Santisteban, L.M., J. Casalí, and J.J. López. 2006. Assessing soil erosion rates in cultivated areas of Navarre (Spain). Earth Surf. Process. Landforms 31(4):487-506.

Deasy, C., S.A. Baxendale, A.L. Heathwaite, G. Ridall, R. Hodgkinson, and R.E. Brazier. 2011. Advancing understanding of runoff and sediment transfers in agricultural catchments through simultaneous observations across scales. Earth Surf. Process. Landforms 36(13):1749-1760.

Di Stefano, C., and V. Ferro. 2011. Measurements of rill and gully erosion in Sicily. Hydrol. Process. 25(14):2221-2227.

Environmental Systems Research Institute (ESRI). 2010. ArcMap desktop: Release 10.0. Redlands, CA.

Eos Systems Inc. 2014. PhotoModeler Scanner (64-bit). Eos Systems Inc., Vancouver, British Columbia.

Faeth, P. 1993. Evaluating agricultural policy and the sustainability of production systems: An economic framework. J. Soil Water Conserv. 48(2):94-99.

Flanagan, D.C., J.C. Ascough II, A.D. Nicks, M.A. Nearing, and J.M. Laflen. 1995. Chapter 1: Overview of the WEPP erosion prediction model. In: USDA-Water Erosion Prediction Project hillslope profile and watershed model documentation,

NSERL Report No. 10. USDA-Agricultural Research Service, West Lafayette, IN.

Gee, G.W., and D. Or . 2002. Particle-size analysis. In: H. Dane and G.C. Topp, editors, Methods of soil analysis: Part 4 physical methods. Soil Science Society of America, Madison, WI. p. 255-293.

Gessesse, G.D., H. Fuchs, R. Mansberger, A. Klik, and D.H. Rieke-Zapp. 2010. Assessment of erosion, deposition and rill development on irregular soil surfaces using close range digital photogrammetry. Photogramm. Rec. 25(131):299-318.

Giménez, R., I. Marzolff, M.A. Campo, M. Seeger, J.B. Ries, J. Casalí, and J. Álvarez-Mozos. 2009. Accuracy of high-resolution photogrammetric measurements of gullies with contrasting morphology. Earth Surf. Process. Landforms 34(14):1915-1926.

Gómez-Gutiérrez, A., S. Schnabel, F. Berenguer-Sempere, F. Lavado-Contador, and J. Rubio-Delgado. 2014. Using 3D photo-reconstruction methods to estimate gully headcut erosion. Catena 120:91-101.

Gordon, L.M., S.J. Bennett, R.L. Bingner, F.D. Theurer, and C.V. Alonso. 2007. Simulating ephemeral gully erosion in AnnAGNPS. Trans. ASABE 50(3):857-866.

Gordon, L.M., S.J. Bennett, C.V. Alonso, and R.L. Bingner. 2008. Modeling long-term soil losses on agricultural fields due to ephemeral gully erosion. J. Soil Water Conserv. 63(4):173-181.

Gordon, L.M., S.J. Bennett, and R.R. Wells. 2012. Response of a soil-mantled experimental landscape to exogenic forcing. Water Resour. Res. 48:W10514. doi:10.1029/2012WR012283

Grossman, R.B., and T.G. Reinsch. 2002. Bulk density and linear extensibility. In: H. Dane and G.C. Topp, editors, Methods of soil analysis: Part 4 physical methods. Soil Science Society of America, Madison, WI. p. 201-228.

Helmers, M.J., X. Zhou, H. Asbjornsen, R. Kolka, M.D. Tomer, and R.M. Cruse. 2012. Sediment removal by prairie filter strips in row-cropped ephemeral watersheds. J. Environ. Qual. 41(5):1531-1539.

Heng, B.C.P., J.H. Chandler, and A. Armstrong. 2010. Applying close range digital photogrammetry in soil erosion studies. Photogramm. Rec. 25(131):240-265.

Kaiser, A., F. Neugirg, G. Rock, C. Müller, F. Haas, J. Ries, and J. Schmidt. 2014. Small-scale surface reconstruction and volume calculation of soil erosion in complex

Moroccan gully morphology using structure from motion. Remote Sens. 6(8):7050-7080. doi:10.3390/rs6087050

Laflen, J.M., D.C. Flanagan, and B.A. Engel. 2004. Soil erosion and sediment yield prediction accuracy using WEPP. J. Am. Water Resour. Assoc. 40(2):289-297.

Lal, R. 2001. Soil degradation by erosion. Land Degrad. Dev. 12(6):519-539.

Leatherman, S.P. 1987. Field measurement of microtopography. J. Coastal Res. 3(2):233-235.

Lentz, R.D., R.H. Dowdy, and R.H. Rust. 1993. Soil property patterns and topographic parameters associated with ephemeral gully erosion. J. Soil Water Conserv. 48(4):354-361.

Lowe, D.G. 2004. Distinctive image features from scale-invariant keypoints. Int. J. Comput. Vis. 60(2):91-110.

Martínez-Casasnovas, J.A., M. Concepción Ramos, and M. Ribes-Dasi. 2005. On-site effects of concentrated flow erosion in vineyard fields: some economic implications. Catena 60(2):129-146.

Marzolff, I., and J. Poesen. 2009. The potential of 3D gully monitoring with GIS using high-resolution aerial photography and a digital photogrammetry system. Geomorphology 111(1-2):48-60.

Momm, H.G., R.L. Bingner, R.R. Wells, and S.M. Dabney. 2011. Application of ground-based LIDAR for gully investigation in agricultural landscapes. ASPRS 2011 Annual Conference Proceedings, Milwaukee, WI.

Momm, H.G., R.L. Bingner, R.R. Wells, and D. Wilcox. 2012. AGNPS GIS-based tool for watershed-scale identification and mapping of cropland potential ephemeral gullies. Appl. Eng. Agric. 28(1):17-29.

Momm, H.G., R.L. Bingner, R.R. Wells, J.R. Rigby, and S.M. Dabney. 2013. Effect of topographic characteristics on compound topographic index for identification of gully channel initiation locations. Trans. ASABE 56(2):523-537.

Nachtergaele, J., and J. Poesen. 1999. Assessment of soil losses by ephemeral gully erosion using high-altitude (stereo) aerial photographs. Earth Surf. Process. Landforms 24(8):693-706.

Nachtergaele, J., J. Poesen, A. Steegen, I. Takken, L. Beuelinck, L. Vandekerckhove, and G. Govers. 2001. The value of a physically based model versus and empirical approach in the prediction of ephemeral gully erosion for loess-derived soils. Geomporhology 49(3-4):237-252.

Nimmo, J.R., and K.S. Perkins. 2002. Aggregate stability and size distribution. In: H. Dane and G.C. Topp, editors, Methods of soil analysis: Part 4 physical methods. Soil Science Society of America, Madison, WI. p. 317-328.

Nouwakpo, S.K., and C. Huang. 2012. A simplified close-range photogrammetric technique for soil erosion assessment. Soil Sci. Soc. Am. J. 76(1):70-84.

Poesen, J.W., J. Boradman, B. Wilcox, and C. Valentin. 1996. Water erosion monitoring and experimentation for global change studies. J. Soil Water Conserv. 51(5):386-390.

Poesen, J. J. Nachtergaele, G. Verstraeten, and C. Valentin. 2003. Gully erosion and environmental change: importance and research needs. Catena 50(2-4):91-133.

Rieke-Zapp, D.H., and M.A. Nearing. 2005. Digital close range photogrammetry for measurement of soil erosion. Photogramm. Rec. 20(109):69-8.

Spomer, R.G., and A.T. Hjelmfelt. 1986. Concentrated flow erosion on conventional and conservation tilled watersheds. Trans. ASAE 29(1):124-127,134.

Stroosnijder, L. 2005. Measurement of erosion: Is it possible? Catena 64(2-3):162-173.

Taylor, J.R. 1997. An introduction to error analysis: The study of uncertainties in physical measurements. University Science Books, Sausalito, CA.

Thomas, A.W., R. Welch, and T.R. Jordan. 1986. Quantifying concentrated-flow erosion on cropland with aerial photogrammetry. J. Soil Water Conserv. 41(4):249-252.

Uri, N.D. 2000. Agriculture and the environment – the problem of soil erosion. J. Sustain. Agric. 16(4):71-94.

USDA -Agricultural Research Service (USDA-ARS). 2013. Science documentation: Revised Universal Soil Loss Equation version 2 (RUSLE 2). USDA-Agricultural Research Service, Washington, DC.

University of Utah Department of Atmospheric Sciences (UUDAS). 2014. MesoWest. http://mesowest.utah.edu (accessed 18 November 2014).

Valcárcel, M., M. Taboada, A. Paz, and J. Dafone. 2003. Ephemeral gully erosion in northwestern Spain. Catena 50(2-4):199-216.

Valentin, C., J. Poesen, and Y. Li. 2005. Gully erosion: Impacts, factors and control. Catena 63(2-3):132-153.

Vandaele, K., J. Poesen, G. Govers, and B. van Wesemael. 1996. Geomorphic threshold conditions for ephemeral gully incision. Geomorphology 16(2):161-173.

Wells, R.R., C.V. Alonso, and S.J. Bennett. 2009. Morphodynamics of headcut development and soil erosion in upland concentrated flows. Soil Sci. Soc. Am. J. 73(2):521-530.

Wells, R.R., S.J. Bennett, and C.V. Alonso. 2010. Modulation of headcut soil erosion in rills due to upstream sediment loads. Water Resour. Res. 46:W12531.

Wells, R.R., H.G. Momm, J.R. Rigby, S.J. Bennett, R.L. Bingner, and S.M. Dabney. 2013. An empirical investigation of gully widening rates in upland concentrated flows. Catena 101:114-121.

Wells, R.R., H.G. Momm, K.R. Gesch, S.M. Dabney, and R.M. Cruse. Quantification of ephemeral gully erosion in Iowa farm fields. In prep.

Woodward, D.E. 1999. Method to predict cropland ephemeral gully erosion. Catena 37(3-4):393-399.

Wu, Y., Q. Zheng, Y. Zhang, B. Liu, H. Cheng, and Y. Wang. 2008. Development of gullies and sediment production in the black soil region of northeastern China. Geomorphology 101(4):683-691.

Zhang, Y., Y. Wu, B. Liu, Q. Zheng, and J. Yin. 2007. Characteristics and factors controlling the development of ephemeral gullies in cultivated catchments of black soil region, Northeast China. Soil Tillage Res. 96(1-2):28-41.

Table 1. 2013 and 2014 counts and dates of photography for sites monitored for ephemeral gully development in 12 experimental watersheds at Neal Smith National Wildlife Refuge (Basswood, B; Interim, I; Orbweaver, O).

Field	Sites monitored		Dates photographed (MM-DD)	
	2013	2014	2013	2014
B1	5	5	06-10	05-14, 05-29, 06-05
B2	2	2	06-10	05-14, 05-29, 06-05
B3	2	2	06-10	05-14, 05-29, 06-05
B4	9	3	06-10	05-14, 05-29, 06-05
B5	8	5	06-10	05-14, 05-29, 06-05
B6	10	10	06-10	05-14, 05-29, 06-05
I1	17	15	06-10	05-14, 05-29, 06-05
I2	12	12	06-10, 09-24	05-14, 05-29, 06-05
I3	10	8	04-22, 06-10, 09-24	05-14, 05-29, 06-05
O1	8	8	04-25, 06-10, 09-24	05-14, 05-29, 06-05
O2	6	6	04-25, 06-10, 09-24	05-14, 05-29, 06-05
O3	10	12	04-25, 06-10, 09-24	05-14, 05-29, 06-05

Table 2. Topographic characteristics (slope, S; area, A; maximum slope length, L_{max}) of the 12 experimental watersheds (Helmers et al., 2012). Ephemeral gully (EG) development occurred in nine of 12 fields.

Field	S (m m^{-1})	A (ha)	L_{max} (m)	EG?	EG length (m)	EG density (m ha^{-1})
B1	0.075	0.53	120	yes	30.4	57.4
B2	0.066	0.48	113	no	-	-
B3	0.064	0.47	110	no	-	-
B4	0.082	0.55	118	yes	19.5	35.5
B5	0.089	1.24	144	yes	18.9	15.3
B6	0.105	0.84	140	yes	62.6	74.5
I1	0.077	3.00	288	yes	102.1	34.0
I2	0.061	3.19	284	yes	137.2	43.0
I3	0.093	0.73	137	yes	63.7	87.3
O1	0.103	1.18	187	yes	61.2	51.9
O2	0.067	2.40	220	no	-	-
O3	0.066	1.24	230	yes	70.9	57.2

Table 3. Bulk density (ρ_b) averaged by block, with uncertainty of two standard deviations (2σ).

Block	Average $\rho_b \pm 2\sigma$ (Mg m^{-3})	
	2013	2014
Basswood	1.32 (0.18)	1.13 (0.22)
Interim	1.24 (0.24)	1.08 (0.21)
Orbweaver	1.30 (0.18)	1.14 (0.25)

Table 4. Soil properties measured from composite samples obtained in Basswood 1, Interim 3, and Orbweaver 1 at five locations (Loc.): in channel at bottom (C_b), in channel at top (C_t), gully bank at bottom (B_b), gully bank at top (B_t), and control (Con). Measured bulk density (ρ_b), texture, total soil carbon (Total C), soil organic matter (OM), and wet aggregate stability (WAS, expressed as percent stable aggregates) values were averaged by location in order to contrast channel (Chan.) with bank, to contrast bottom (Bot.) with top, and for comparison against the control (Con).

Block	Loc.	ρ_b (Mg m^{-3})	Sand (%)	Silt (%)	Clay (%)	Total C (%)	OM (%)	WAS (%)
Basswood	C_b	1.13	5.48	66.70	27.82	2.10	3.9	27.6
	C_t	1.16	5.74	66.83	27.43	1.65	3.1	27.2
	B_b	1.08	5.12	70.22	24.66	1.97	3.7	19.5
	B_t	1.21	3.54	70.66	25.80	2.07	3.9	25.0
	Con	1.26	2.92	67.04	30.04	2.28	4.3	28.4
Interim	C_b	1.21	20.34	51.16	28.50	1.61	3.0	24.6
	C_t	1.27	14.36	56.11	29.53	1.24	2.4	27.9
	B_b	1.22	19.82	51.09	29.09	1.69	3.2	29.9
	B_t	1.06	14.51	55.45	30.04	1.90	3.6	25.9
	Con	1.18	12.23	54.96	32.81	2.26	4.2	48.5
Orbweaver	C_b	1.20	17.21	56.00	26.79	2.36	4.4	22.7
	C_t	1.09	7.52	64.14	28.34	2.68	5.0	36.5
	B_b	1.30	14.14	58.71	27.15	2.61	4.9	29.7
	B_t	1.06	8.06	63.87	28.07	2.81	5.2	32.5
	Con	1.15	22.05	52.74	25.21	2.41	4.5	51.3
Overall	Chan.	1.18	11.78	60.16	28.07	1.94	3.63	27.75
	Bank	1.15	10.87	61.67	27.47	2.17	4.08	27.08
	Bot.	1.19	13.69	58.98	27.34	2.05	3.85	25.66
	Top	1.14	8.96	62.84	28.20	2.06	3.87	29.16
	Con	1.20	12.40	58.25	29.35	2.31	4.33	42.72

Table 5. Net volume loss (ΔV_c), net sediment efflux (ΔM), net sediment efflux per channel area, and net sediment efflux per watershed area for three watersheds at Neal Smith National Wildlife Refuge (Interim, I; Orbweaver, O) during the time interval April 25, 2013 to June 10, 2013: T_0 to T_1. Parenthetical values for ΔV_c and ΔM are 2σ uncertainties $\delta\Delta V_c$ and $\delta\Delta M$, respectively. Negative values indicate positive volume change (net sediment deposition). Asterisk indicates insignificant tabulated values due to the uncertainty being larger in magnitude than calculated values of volume change and sediment flux.

Field	ΔV_c (m^3)	ΔM (Mg)	Erosion	
			Per channel (Mg ha^{-1})	Per field (Mg ha^{-1})
I3	3.821 (0.146)	4.733 (0.921)	418.670	6.484
O1*	–0.073 (0.142)	–0.094 (0.185)	–8.586	–0.080
O3	1.314 (0.114)	1.706 (0.282)	193.530	1.376

Table 6. Net volume loss (ΔV_c), net sediment efflux (ΔM), net sediment efflux per channel area, and net sediment efflux per watershed area for four watersheds at Neal Smith National Wildlife Refuge (Interim, I; Orbweaver, O) during the time interval June 10, 2013 to September 24, 2013: T_1 to T_2. Parenthetical values for ΔV_c and ΔM are 2σ uncertainties $\delta\Delta V_c$ and $\delta\Delta M$, respectively. Negative values indicate positive volume change (net sediment deposition).

Field	ΔV_c (m^3)	ΔM (Mg)	Erosion	
			Per channel (Mg ha^{-1})	Per field (Mg ha^{-1})
I2	2.387 (0.293)	2.956 (0.670)	130.895	0.927
I3	1.514 (0.146)	1.875 (0.401)	165.844	2.568
O1	–0.640 (0.142)	–0.830 (0.218)	–75.682	–0.704
O3	0.571 (0.114)	0.741 (0.181)	84.037	0.597

Table 7. Net volume loss (ΔV_c), net sediment efflux (ΔM), net sediment efflux per channel area, and net sediment efflux per watershed area for eight watersheds at Neal Smith National Wildlife Refuge (Basswood, B; Interim, I; Orbweaver, O) during the time interval May 14, 2014 to May 29, 2014: T_3 to T_4. Parenthetical values for ΔV_c and ΔM are 2σ uncertainties $\delta\Delta V_c$ and $\delta\Delta M$, respectively. Negative values indicate positive volume change (net sediment deposition). Asterisks indicate insignificant tabulated values due to the uncertainties being larger in magnitude than calculated values of volume change and sediment flux.

Field	ΔV_c (m^3)	ΔM (Mg)	Erosion	
			Per channel (Mg ha^{-1})	Per field (Mg ha^{-1})
B1	0.132 (0.072)	0.149 (0.086)	26.973	0.281
B4*	0.042 (0.044)	0.048 (0.050)	14.118	0.087
B5	0.284 (0.043)	0.321 (0.080)	95.899	0.259
B6	0.515 (0.138)	0.581 (0.193)	54.663	0.692
I1	0.843 (0.230)	0.911 (0.305)	51.292	0.304
I2	0.518 (0.317)	0.560 (0.359)	22.911	0.176
I3	0.526 (0.143)	0.569 (0.190)	51.363	0.780
O3*	–0.002 (0.156)	–0.003 (0.178)	–0.210	–0.002

Table 8. Net volume loss (ΔV_c), net sediment efflux (ΔM), net sediment efflux per channel area, and net sediment efflux per watershed area for eight watersheds at Neal Smith National Wildlife Refuge (Basswood, B; Interim, I; Orbweaver, O) during the time interval May 29, 2014 to June 5, 2014: T_4 to T_5. Parenthetical values for ΔV_c and ΔM are 2σ uncertainties $\delta\Delta V_c$ and $\delta\Delta M$, respectively. Negative values indicate positive volume change (net sediment deposition). Asterisk indicates insignificant tabulated values due to the uncertainty being larger in magnitude than calculated values of volume change and sediment flux.

Field	ΔV_c (m^3)	ΔM (Mg)	Erosion	
			Per channel (Mg ha^{-1})	Per field (Mg ha^{-1})
B1	–0.526 (0.072)	–0.594 (0.142)	–107.496	–1.120
B4*	0.036 (0.044)	0.041 (0.050)	12.117	0.075
B5	–0.118 (0.043)	–0.133 (0.055)	–39.701	–0.107
B6	–0.220 (0.138)	–0.249 (0.163)	–23.401	–0.296
I1	–1.063 (0.230)	–1.150 (0.334)	–64.730	–0.383
I2	–0.520 (0.317)	–0.562 (0.359)	–22.970	–0.176
I3	–0.700 (0.143)	–0.757 (0.213)	–68.374	–1.038
O3	–0.360 (0.156)	–0.412 (0.199)	–34.236	–0.332

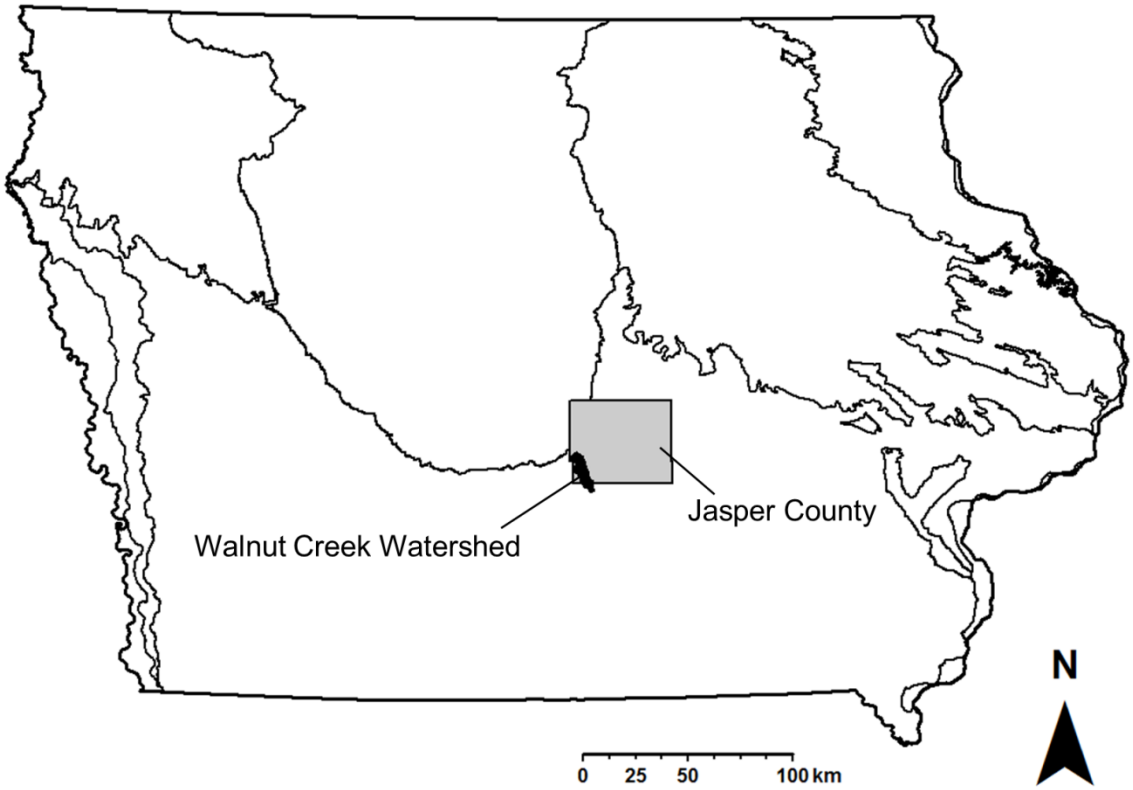

Figure 1. Study site was located at Neal Smith National Wildlife Refuge, which is within the Walnut Creek Watershed in southwest Jasper County, Iowa, USA.

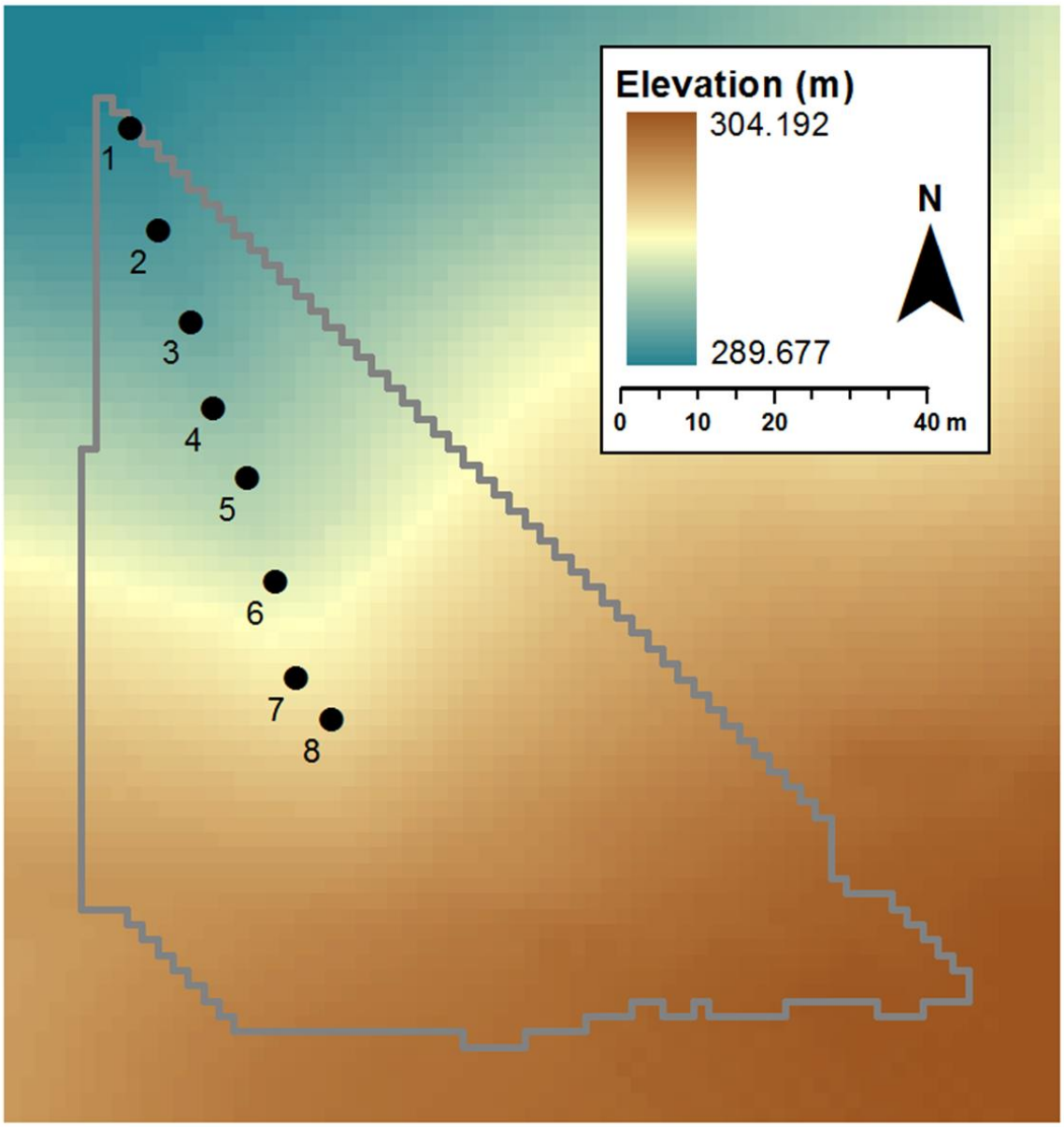

Figure 2. Eight monitoring sites (black dots) placed sequentially along the concentrated flowpath in Interim 3. The gray outline is the boundary of the field, which is a zero-order watershed.

Figure 3. Each monitoring site was delineated by a set of four survey stakes, which were located with a 1.8 m by 1.2 m PVC frame. Stakes were surveyed for future use as ground control points during photogrammetric point cloud generation and post-processing.

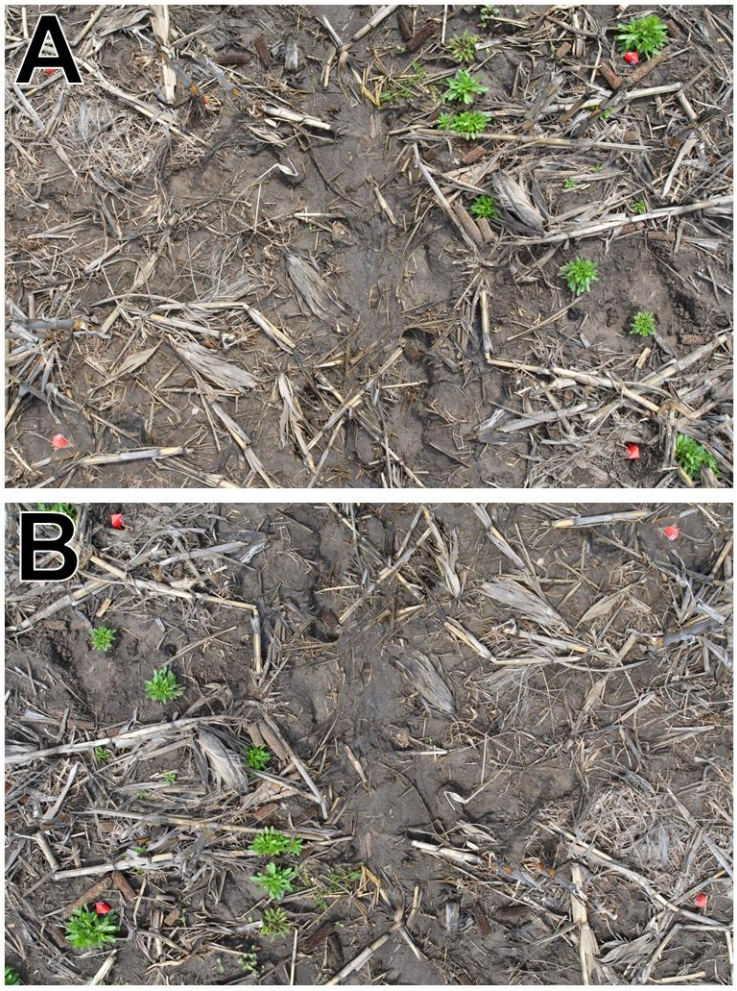

Figure 4. A. Upstream facing image at Interim 3 Site 6 for T_0 (April 22, 2013). B. Downstream facing image at Interim 3 Site 6 for T_0.

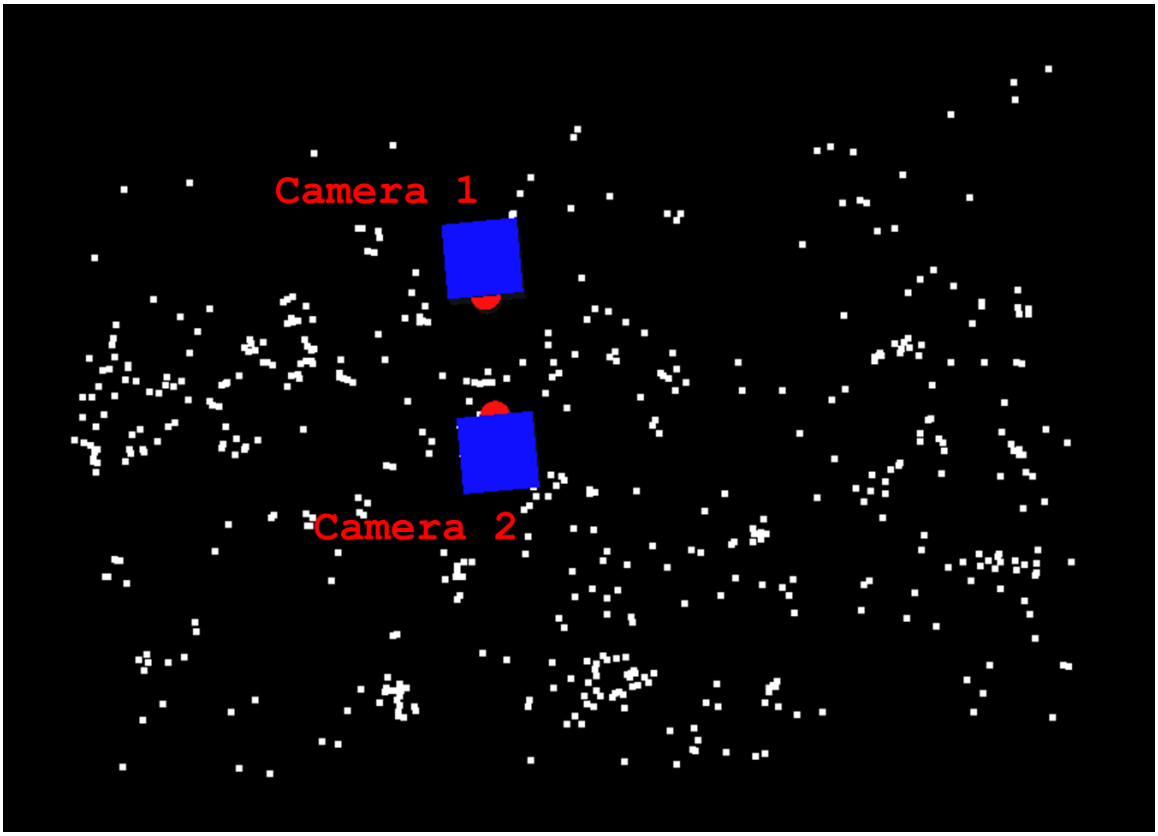

Figure 5. Matching points (white dots) and camera sensors automatically located by PhotoModeler Scanner using as input the image pair shown in Figure 4 of Interim 3 Site 6 from T_0 (April 22, 2013).

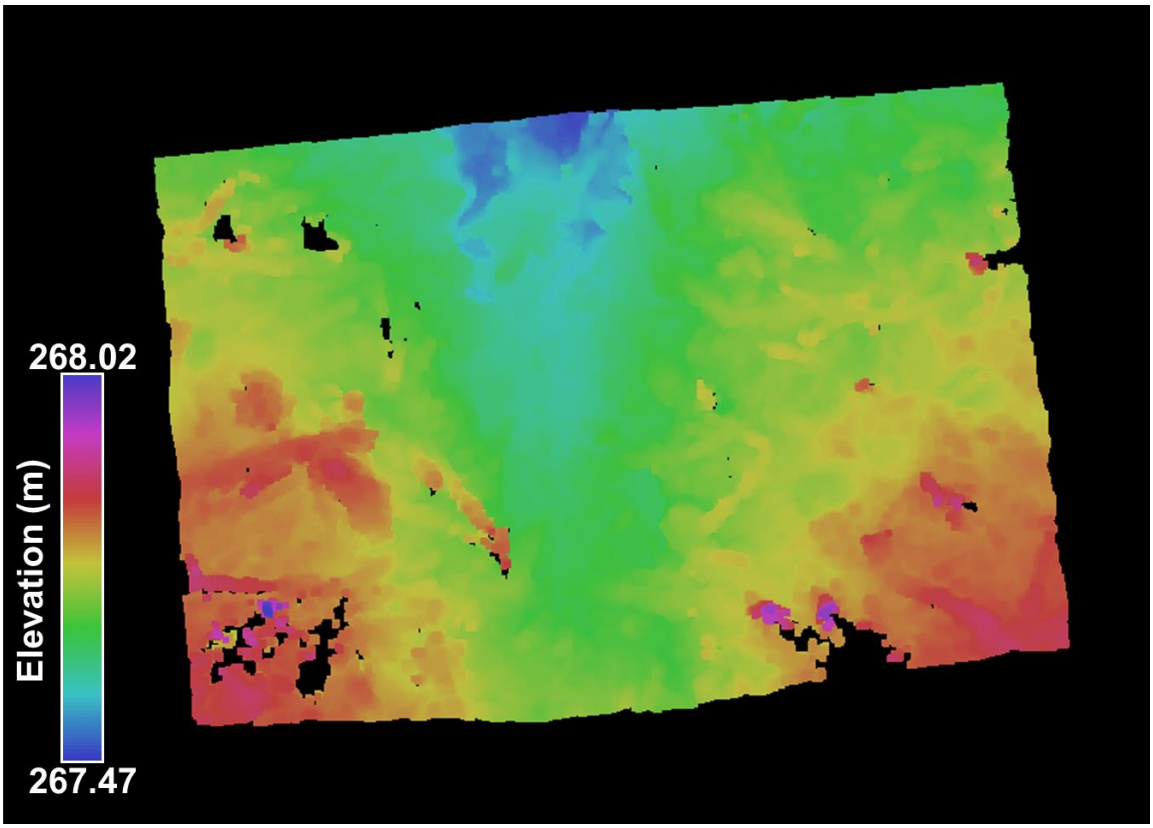

Figure 6. Point cloud for Interim 3 Site 6 at T_0 (April 22, 2013) generated with PhotoModeler Scanner.

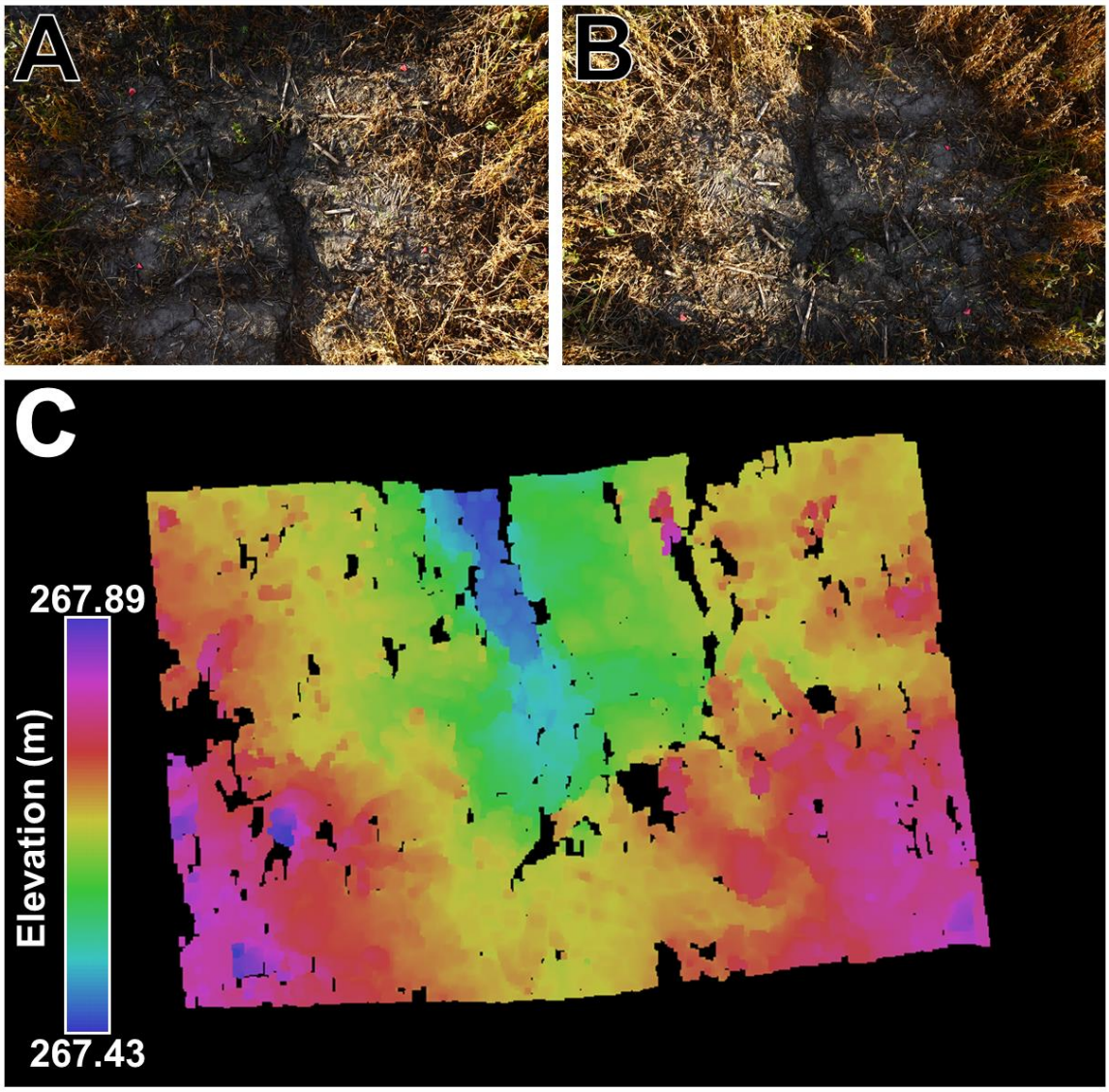

Figure 7. A. Upstream facing image at Interim 3 Site 6 for T_2 (September 24, 2013). B. Downstream facing image at Interim 3 Site 6 for T_2. C. Point cloud for Interim 3 Site 6 at T_2 generated with PhotoModeler Scanner.

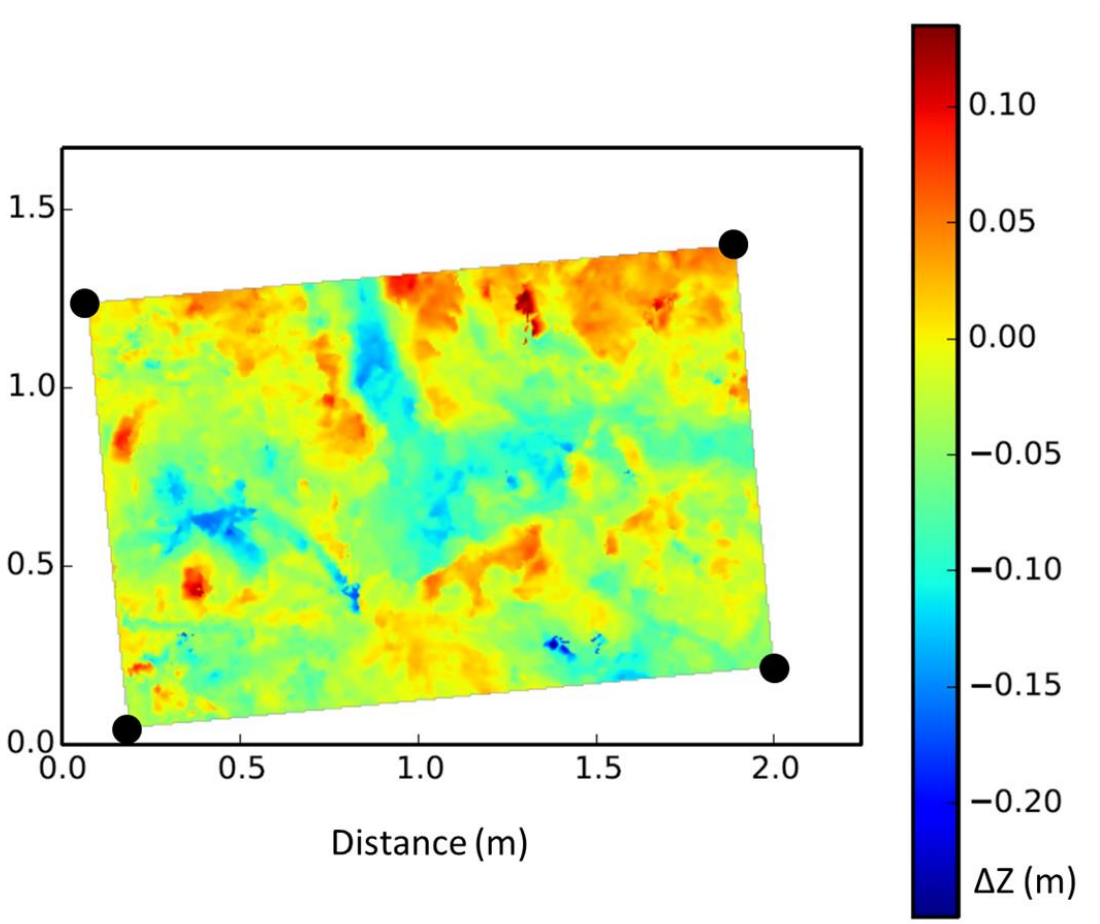

Figure 8. Elevation changes within Interim 3 Site 6 between T_0 (April 22, 2013) and T_2 (September 24, 2013). Elevation changes in all raster cells are used to determine volume change (Chapter 2 Equation 1), which was –0.063649 m^3 over the time interval T_0 to T_2.

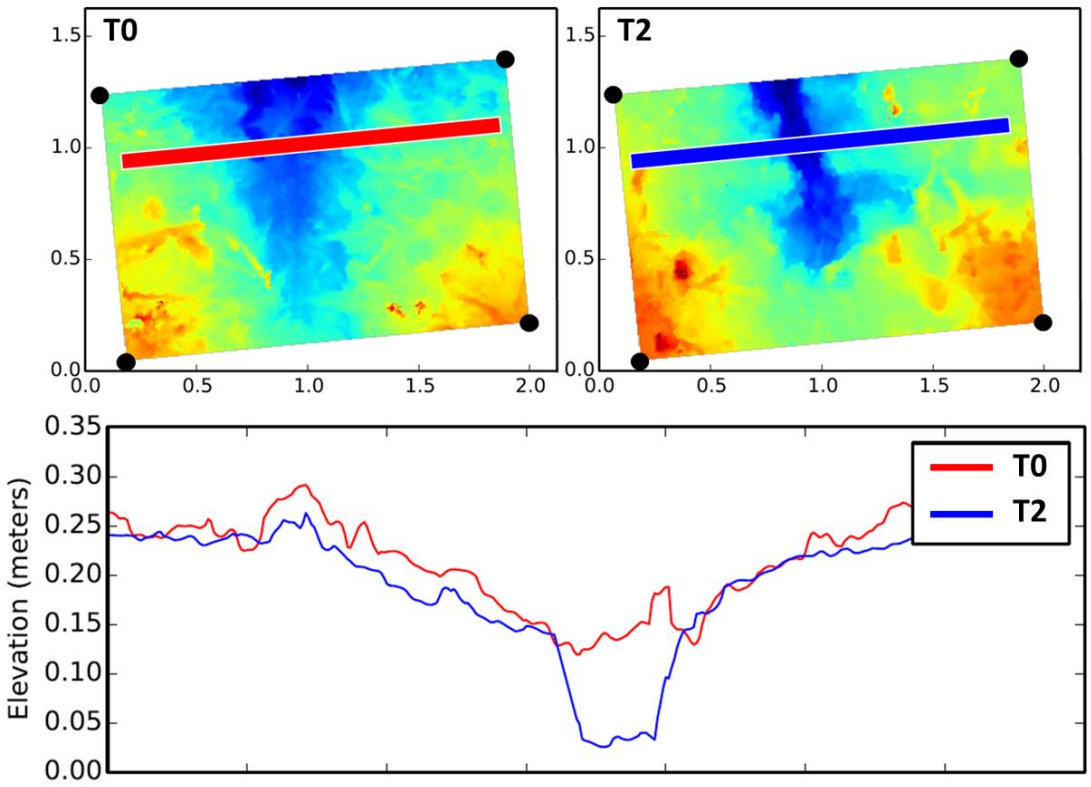

Figure 9. Cross-section profiles extracted from the T0 (red) and T2 (blue) point clouds during post-processing. This is a graphical representation of the data contained in the *.csv tables of ephemeral gully morphologies.

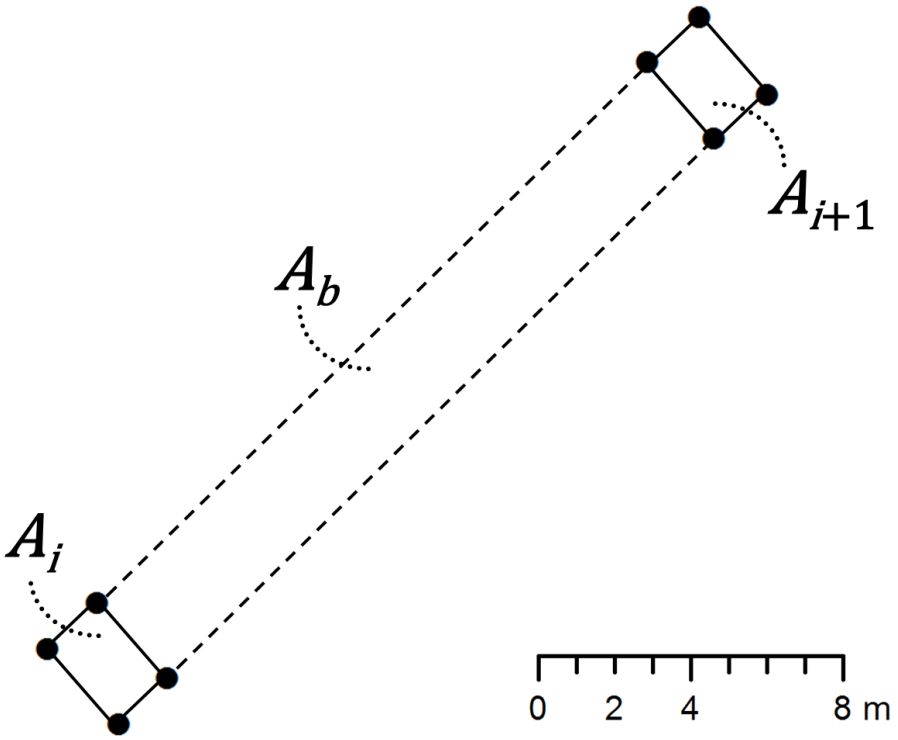

Figure 10. Example of the interpolation procedure used in Equation 2, which is a modification of the end area method. Interim 2 Site 5 area (A_i) and Interim 2 Site 6 area (A_{i+1}) are used to determine the average elevation change in the area between the sites (A_b). Average elevation change within each segment (Site 5, Site 6, and between) are multiplied by the corresponding areas (A_i, A_{i+1}, and A_b) to determine the volume of each segment, and all segment volumes are summed to calculate total volume change for an entire ephemeral gully.

CHAPTER 4

EPHEMERAL GULLY EROSION AND SOIL CONSERVATION

Soil erosion is a losing proposition for many sectors of society. Agricultural producers lose income through yield declines and loss of agronomic inputs such as fertilizers. Landowners see their assets depreciate due to soil degradation. Off-farm stakeholders bear the economic burden of externalities imposed by erosion-related damages such as reservoir sedimentation and increased flooding. Ephemeral gully erosion is a particularly problematic type of soil loss as it exacerbates off-site negative consequences because these channels serve as links between agricultural catchments and downstream ecosystems. Because ephemeral gullies are disproportionately large pollution sources, soil conservation practices that specifically target their formation and evolution can lead to disproportionately large economic and ecological benefits.

Soil erosion models are one tool available to conservationists. A suite of models that encompass a variety of scales (e.g. individual ephemeral gully, separate field, entire watershed) can be used to allocate limited financial and human capital for maximum conservation (Momm et al., 2013). Watershed modeling can give spatial insights for gully erosion susceptibility, single channel models can be used to simulate the physical processes of channel erosion (e.g. incision, headcut migration, channel widening), and the intermediate approach of field-scale modeling can be leveraged to design and evaluate conservation practices to control ephemeral gully erosion. A model is a simplification of reality, and its quality is dependent upon the data on which it is based. Soil erosion models must be validated with field measurements (Poesen et al., 1996). In this research

project, a photogrammetric approach developed by Wells et al. (in prep.) was validated and applied for quantification of ephemeral gully erosion.

Validation of the field measurement technique was performed to quantify the accuracy of the data obtained. Accuracy was assessed by calculation of measurement uncertainty, which was defined by precision. Two times the standard deviation of a population of volume changes between replicated digital elevation models of an experimental surface was used as the metric of uncertainty in average elevation change between two surfaces. The small uncertainty, along with the high relative vertical accuracy of a single digital surface reconstruction and acceptable absolute accuracy of geo-referenced point clouds, indicates that close-range photogrammetry provides a viable method to detect morphological changes within ephemeral gullies.

Application of the validated technique to experimental watersheds revealed that observation-scale geomorphic change data were reasonable when extrapolated to the scale of entire fields. The multi-temporal morphological ephemeral gully data gathered and generated address the documented need for more field measurements of ephemeral gully erosion (Dabney et al., 2011). A dataset of soil parameters was also compiled to complement gully topographic data. Plant growth interfered with photogrammetry, but otherwise the method was successfully applied to generate a useful database for future improvement of predictive ephemeral gully erosion models.

This study could be improved by accounting for dynamic soil properties, especially bulk density. Measurement of soil properties at greater spatial and temporal resolutions would allow for better parameterization of erosion models and might improve statistical relationships between soil and ephemeral gullying. More complex terrain

indices could yield better insights into landscape-gully relationships. One associated consequence of ephemeral gully erosion that merits further exploration is phosphorus (P) transport. Within no-till management systems (i.e. stratified soil P concentration) in particular, P movement due to ephemeral gully erosion and concentrated runoff should be quantified.

While the field data generated in this study can benefit soil erosion models that may eventually be used for soil conservation planning, predictive models alone will not curtail ephemeral gully erosion. Innovative conservation practices can dramatically lower sediment export from agricultural land (e.g. Helmers et al., 2012). In addition to creativity, a firm commitment to soil conservation as an international economic and agroecological priority will be needed to protect this vital natural resource. Holistic accounting for the long-term financial and biophysical impacts of soil erosion is necessary to maintain the inherent production potential of soil (Cruse et al., 2013). Adequate valuation and conservation of this fragile and dynamic resource are needed to achieve and sustain the maximum natural and societal services provisioned by healthy soil.

References

Cruse, R.M., S. Lee, T.E. Fenton, E. Wang, and J. Laflen. 2013. Soil renewal and sustainability. In: R. Lal and B.A. Stewart, editors, Principles of sustainable soil management in agroecosystems. CRC Press, Boca Raton, FL. p. 477-500.

Dabney, S.M., D.C. Yoder, D.A.N. Vieira, and R.L. Bingner. 2011. Enhancing RUSLE to include runoff-driven phenomena. Hydrol. Process. 25(9):1373-1390.

Helmers, M.J., X. Zhou, H. Asbjornsen, R. Kolka, M.D. Tomer, and R.M. Cruse. 2012. Sediment removal by prairie filter strips in row-cropped ephemeral watersheds. J. Environ. Qual. 41(5):1531-1539.

Momm, H.G., R.L. Bingner, R.R. Wells, J.R. Rigby, and S.M. Dabney. 2013. Effect of topographic characteristics on compound topographic index for identification of gully channel initiation locations. Trans. ASABE 56(2):523-537.

Poesen, J.W., J. Boradman, B. Wilcox, and C. Valentin. 1996. Water erosion monitoring and experimentation for global change studies. J. Soil Water Conserv. 51(5):386-390.

Wells, R.R., H.G. Momm, K.R. Gesch, S.M. Dabney, and R.M. Cruse. Quantification of ephemeral gully erosion in Iowa farm fields. In prep.